Thermal performance of a phase change material-based heat sink in presence of nanoparticles and metal-foam to enhance cooling performance of electronics

Adeel Arshad[a,*], Mark Jabbal[a], Hamza Faraji[b], Pouyan Talebizadehsardari[c], Muhammad Anser Bashir[d], Yuying Yan[a,*]

[a]*Fluids & Thermal Engineering (FLUTE) Research Group, Faculty of Engineering, University of Nottingham, Nottingham, NG7 2RD, UK*
[b]*Physics Department, LPMMAT Laboratory, Faculty of Sciences Ain Chock, Hassan II University, Casablanca, Morocco*
[c]*Department of Mechanical and Aerospace Engineering, Institute of Energy Futures, Brunel University London, Uxbridge, Middlesex UB8 3PH, UK*
[d]*Department of Mechanical Engineering, Mirpur University of Science & Technology (MUST), Mirpur 10250, AJK, Pakistan*

Abstract

The present study explores the parametric investigation of a heat sink filled with composite of pure phase change material (PCM), nanocomposite phase change material (NCPCM), metal-foam (MF) by employing the numerical approach for effective passive thermal management of electronics. The combinations of heat sink are varied by filling PCM, NCPCM, MF+PCM and NCPCM+MF. Different parameters such as MF materials, porosities, pore densities (PPI-pores per inch), volume fractions of nanoparticles in NCPCM, power levels and combination of MF+NCPCM by varying different porosities and nanoparticles volume fractions. Copper (Cu) nanoparticles of 1%, 3% and 5% volume fraction were dispersed in RT–35HC, used as a PCM, and copper, aluminium (Al) and nickel (Ni) MFs were embedded inside the heat sink. Transient simulations with conjugate heat transfer and melting/solidification schemes were formulated using finite–volume–method (FVM). The thermal performance and melting process of the NCPCM filled heat sink were evaluated through melting time, heat storage capacity, heat storage density, rate of heat transfer and rate of heat transfer density. The results showed that with the addition of Cu nanoparticles and MF, the rate of heat transfer was increased and melting time was reduced. The melting time was reduced by -1.25%, -1.87% and -2.34%; and rate of heat storage is enhanced

---

*Correspondence authors

Email addresses: adeel.arshad@nottingham.ac.uk, adeel_kirmani@hotmail.com (Adeel Arshad), yuying.yan@nottingham.ac.uk (Yuying Yan)

by 1.35%, 0.76%, and 0.19% with the addition of 1%, 3% and 5% volume fraction of Cu nanoparticles, respectively. The composite of MF+NCPCM showed the lower heat sink temperature and higher liquid–fraction were obtained. The latent–heating phase duration was decreased with the increase of Cu nanoparticles volume fraction. Additionally, the lower reduction in melting time of -18.10% and higher rate of heat transfer of 8.12% were obtained with 1% Cu nanoparticles, 95% porosity and 10 PPI Cu MF based heat sink.

1. Introduction

The reliability of smart electronic devices is purely based on their ability to perform the preprogrammed functions under the safe operating conditions. With the advancement in electronics and telecommunications industries, the electronics products have shifted towards lightweight, low power consumption, faster and smaller [1]. Gradually, the growing miniaturization and advanced multi-features of smart electronic devices have led towards the more complexity in thermal management (TM) solutions subjected the medium to high–heat–flux. Internal overheating and rise of the temperature as a result of this, lead to damage or failure of electronic devices around 55% compared with the other failures [2]. Modern TM technologies including active and passive, the active cooling methods such air or liquid cooling, adopted to cool the portable electronic devices have some limitations such as high–power consumption, acoustic noise production, bulk in volume and size [1, 3]. In such instances, a novel technology is needed which can ensure the passive TM in the best possible way. Significant outcomes of cooling through PCMs with heat sink, used as passive heat exchanger, in electronics equipment have been achieved as they emanate heat during heavy usage due to their high latent–heat of fusion with isothermal phase transformation [4]. To facilitate the reliable TM of electronic devices, a latent–heat storage unit (LHSU) containing high thermal conductivity enhancers in form of extruded fins [5–8], metal-foams [9, 10] and nanoparticles [11–13] with PCMs embedded in a heat sink are invariably used [14, 15].

Many researchers have introduced the applications on PCM with porous medium using either metallic foams or carbon material such as expanded graphite integrated with heat sink, heat pipe and shell and tube heat energy storage system. Zhao et al. [16] conducted a experimental study to investigate the heat transfer enhancement through a PCM/MF heat storage system. RT–58 and Cu MF were embedded and melting and solidifying processes were analysed. The results found that using the Cu MF as heat transfer enhancement media, increased the overall heat transfer rate by 3–10 times while phase–change process. Further, Tian and Zhao [17] conducted a numerical study to effect of MFs on heat transfer enhancement using 2D LTNE model and conduction and convection heat transfer modes were considered at phase–transition and liquid–phase. The key findings were reported that heat conduced rate was improved by using the MF because of high thermal conductivity and natural convection effects were suppressed because of the large flow resistance in MF. Sundarram and Li [18] investigated the pore size and porosity of aluminium MFs infiltrated

with paraffin wax as a PCM using a three-dimensional finite element model. The results found that at a constant porosity, the smaller pore size reduced the more heat source temperature for a longer duration compared with higher pore size. In addition, the effective thermal conductivity of MF+PCM system was doubled by reducing the pore size from 100 to 25 μm. Chen et al. [19] conducted a experimental and numerical study using aluminium made MF integrated with paraffin wax at pore scale. Authors studied the temperature field and melting evolution MF+PCM and found that MF had the capability to enhance the phase–change heat transfer during solid–liquid phase transformation due to the thermal conduction in the metal matrix. Nada and his co–authors [20] conducted the comprehensive parametric study by using carbon–foams of varying porosities and thermal conductivities and PCMs of different latent–heat of fusions and melting temperatures at different input heat fluxes. The effects of module thickness and power densities were investigated and the results showed that by decreasing carbon–foam and PCMs thermal conductivities, increasing the module height and carbon–foam porosity increased the module temperature and delayed the steady–state temperature time. Further, the authors used the nano–carbon tubes along with carbon–foam and PCM (RT–65) and the effect of pure carbon–foam, carbon–foam+RT–65 and carbon–foam+RT–65/nano–carbon tubes of different porosities were investigated numerically [21].The results revealed that carbon–foam+RT–65/nano–carbon tubes reduced the 11.5% module surface temperature with less then 75% carbon–foam porosities and a 7.8% reduction was obtained with 88% porosity. Alipanah and Li [22] proposed a numerical study for TM of Li–ion battery by using octadecane, gallium and octadecane+aluminium MF. Three different porosities of 0.88, 0.925 and 0.97 and three heat fluxes of 400, 600, and 800 W/m^2 were varied. The results revealed that octadecane+aluminium MF of 0.8% led to the 7.3 times longer discharge time compared to the pure octadecane case. Furthermore, the addition of aluminium MF increased the uniformity in battery surface temperature. Zhang et al. [23] conducted the experimental and numerical study consisting of Cu MF and paraffin wax in a square cavity for thermal energy storage and TM applications. The phase–change heat transfer and melting phenomenon were studied and found that there was a quite significant difference between the ligament of Cu MF and paraffin wax because of the non–equilibrium thermal effects in heat transfer between the paraffin wax and Cu MF. Mahdi and Nsofor [24, 25] conducted the numerical studies to study the melting and solidification processes in a triplex–tube thermal energy system using Al$_2$O$_3$ nanoparticles and Cu MF combination under three heat transfer fluid temperatures. Three different nanopar-

4

ticles volume fractions of 0.01, 0.03 and 0.05 and two MF porosities of 0.95 and 0.98 were varied for each inlet fluid temperature. The authors found that melting and solidification processes were improved with the addition of MF and nanoparticles further improved the melting and solidification processes with the increase of volume fraction. In addition, the authors reported that with the increase of MF porosity, the potential of nanoparticles for enhancing the thermal energy storage was decreased. Further, the combination of NCPCM and MF was numerically investigated by Bernardo et al. [26] by adding 1% and 5% of Al_2O_3 nanoparticles in RT–58, as a PCM, and aluminium MF having 80% and 90% porosities. The authors revealed that MF improved the charging or discharging rate more significantly of the system instead of the nanoparticles. The nanoparticles could be used to only to adjust the charging or discharging time moderately during phase–transformation processes. Chamkha et al. [27] conducted a numerical study using a L–shape enclosure heat sink consisting of Cu MF and paraffin wax under the pulse heat flux conditions to study the flow and heat transfer phenomenon. A constant and uniform efficiency were obtained by the MF+PCM heat during the pulse heating. The results revealed that the higher pulse heat flux showed that higher heat sink efficiency. The efficiencies of 1.75 and 2.4 were obtained by providing the element heat flux to fourfold and sixfold of the steady heat flux, respectively. Recently, Li et al. [28] conduced a numerical study by using porous/NCPCM system in a counter current triple–tube to explore the effect of MF and NCPCM under different heat transfer fluid temperatures and directions. The results showed that by 5% of Cu nanoparticles, the melting/solidification period was reduced by 25.9%/28.2%. In addition, with 95% porosity of MF, the melting/solidification period was reduced by 83.7%/88.2% which revealed that embedding the MF with PCM had the more advantage than the adding nanoparticles into the PCM.

The aforementioned literature reveals that a few studies have explored the effect of adding nanoparticles into the PCM and MF+PCM specially in an application of latent–heat thermal energy storage system. Therefore, the present study aim to explore the effect of four different heat absorbing mediums such as PCM, NCPCM, MF+PCM and MF+NCPCM filled in a heat sink for passive thermal cooling of electronic devices. The RT–35HC is used as a PCM and copper (Cu) nanoparticles of varying volume fractions are dispersed into the PCM. Three different MFs made of Cu, aluminium (Al), and nickel (Ni) are investigated to find the best heat conductive MF with PCM. Three different porosities, five different pore densities and four different input power levels of 5, 6, 7, and 8 W are varied. Firstly,

the MF of constant porosity is embedded into NCPCM of different volume fractions and secondly, the NCPCM of constant volume fraction is varied with different porosities of MF to explore the effect of two heat conductive mediums. The melting phenomenon and temperature distribution of of pure PCM, NCPCM, MF+PCM and NCPCM+MF based heat sink is studied. Moreover, thermal cooling performance is presented using four different performance evaluation parameters such as heat storage capacity, heat storage density, rate of heat transfer, and rate of heat transfer density along with the total melting time. This will eventually provide a better picture to select the optimum heat storage medium filled in a heat sink for efficient solution of passive thermal cooling of electronic devices.

2. Geometric and Mathematical description

2.1. Physics of the problem

In present study, a two-dimensional (2D) heat sink is considered filled up with the composite of PCM, NCPCM, MF+PCM and MF+NCPCM, as shown in Fig. 1 and the configuration of each case is presented in Fig. 2 investigated in current study. The heat sink with width ($W = 70$ mm) and height ($H = 25$ mm) is heated with a heat source of volumetric heat generation (q''') with sizes of $l = 50$ mm and $t = 2$ mm. All the sides of heat sink are adiabatic except top surface which undergoes with natural convection. The internal cavity of the heat sink has width of $w = 60$ mm and height $h = 20$ mm. The heat sink is made of Cu and numerically modelled to investigate the thermal performance for passive cooling of electronic devices. The effect of different parameters such as different MF materials, porosities, pore densities, volume fractions of nanoparticles in NCPCM, combination of NCPCM+MF by varying different porosities and nanoparticles volume fractions, and power levels. The RT–35HC is used as PCM having melting temperature of 35 °C. Three different volume fractions of $\varphi = 1\%$, 3%, and 5% of Cu nanoparticles are dispersed in RT–35HC to study the effect of NCPCM based heat sink. Three different porosities of 95%, 90%, and 80% and five different pore densities or PPI of 10, 20, 30, 40 and 50 are varied of MF embedded inside the PCM heat sink to study the effect of MF+PCM heat sink. The MFs made of Cu, Al and Ni are investigated with PCM. Five different power levels of 4, 5, 6, 7, and 8 W are provided at the base of heat sink to analyse the temperature distribution and melting phenomenon MF+PCM based heat sink. The 95% porosity and 10 PPI of Cu MF is kept constant with pure PCM and NCPCM of $\varphi = 1\%$, 3%, and 5% heat sink cases. Similarly, NCPCM of 5% volume fraction of Cu nanoparticles is kept constant with pure PCM and MF

6

of 95%, 90%, and 80% porosities to investigate the optimum volume fraction and porosity of composite NCPCM+MF filled heat sink. The current system is designed based on the average dimensions of portable hand–held electronic devices to investigate passive thermal performance using pure PCM, NCPCM, MF+PCM and MF+NCPCM based heat sink.
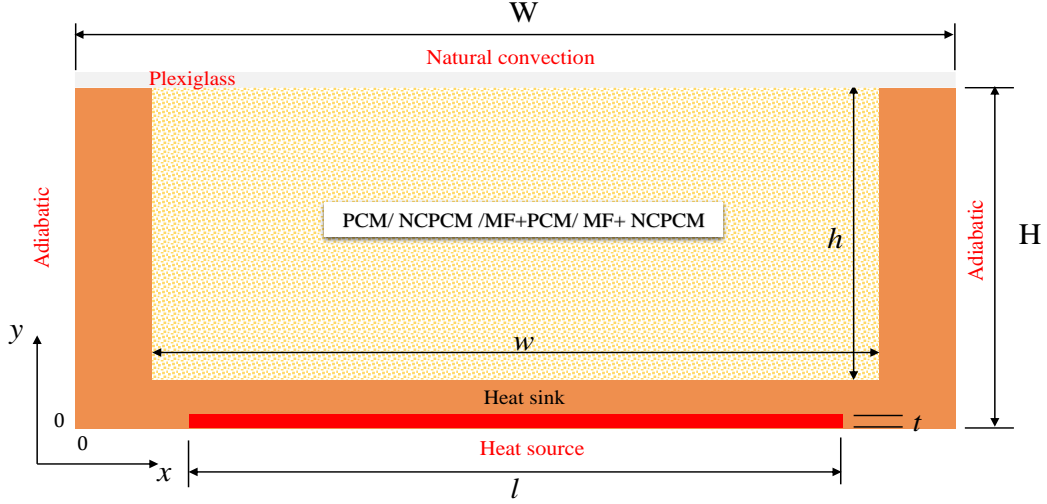
Figure 1: *Schematic diagram of the computational domain used in current study.*

2.2. Mathematical formulation

The governing equations are applied based on the PCM and NCPCM based heat sink embedded with MF, shown in Fig. 1. During melting process of pure PCM and NCPCM, heat is transferred through conduction mode while in solid–phase and then conduction and natural convection modes contribute the heat transfer while generation of liquid–phase due the temperature gradient. Since, the pure PCM has low thermal conductivity, a solid porous medium is embedded inside the PCM and NCPCM which enhances the heat transfer rate by conduction rather than convection because of the high flow–resistant effect of MF structure. Since, the presence of MF increases the volume of heat sink having a similar PCM or NCPCM mass. Moreover, due to the flow–resistant of MF structure, the effect of natural convection is negligible in MF+PCM and NCPCM+MF cases. By adding the nanoparticles into the pure PCM, the thermophysical properties of PCM are changed. The purpose to add the nanoparticles is to modify the thermal conductivity of PCM. The effective density is increased, whereas latent–heat of fusion and specific heat capacity are reduced.

In numerical modelling, the enthalpy–porosity method is adopted to model the effect of phase transformation of pure PCM and NCPCM inside the MF embedded heat sink, where the porosity is equal to the liquid–fraction of each cell. Due the presence of MF, the vis-

7

Case	Configuration
PCM filled heat sink	
NCPCM filled heat sink	
MF+PCM filled heat sink	
MF+NCPCM filled heat sink	
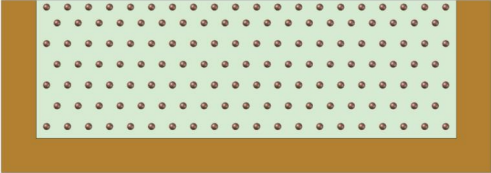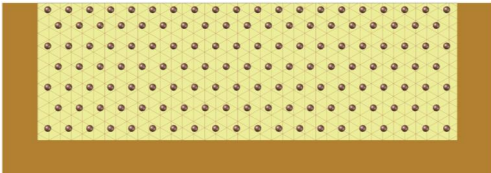
Figure 2: *Different configurations of heat sink investigated in current study.*

cous and inertial losses are overcome by introducing the pressure drop effect in momentum equation. The MF as a porous medium is modelled by considering the Darcy–Forchheimer–Brinkman model (DFBM) and a source term is introduced in momentum equation. The following assumptions are considered to define the continuity, momentum and energy equations [29–31]:

- An open cell MF is assumed homogeneous and isotropic.

- An incompressible, transient, laminar and Newtonian fluid is considered of liquid PCM and NCPCM inside the MF.

- Local thermal equilibrium model is assumed between the PCM, NCPCM and MF in energy equation.

- Volume expansion of PCM and NCPCM is negligible during phase transformation process.

- Viscous dissipation is negligible and no-slip boundary condition are assumed for velocities.

- Constant thermophysical properties are considered for nanoparticles, PCM and NCPCM expect the density for PCM and NCPCM.

- The heat sink is considered as solid–state with homogeneous and isotropic properties and thermal conduction heat transfer exists.

- The Boussinesq approximation is assumed to simulate the buoyancy driven effect under natural convection as $\rho = \rho_m/[\beta(T - T_m) + 1]$, where $T_m = (T_s + T_l)/2$.

- The NCPCM is considered as colloid suspension which exhibits as a Newtonian fluid. The liquid NCPCM flow regime is $2D$, laminar, unsteady and incompressible.

- The dispersion of nanoparticles in PCM is assumed homogeneous, no agglomeration is considered.

- The nanoparticles and PCM are in local thermal equilibrium and there is no–slip between them.

- The initial temperature of heat sink, PCM, NCPCM and MF are the same.

- Adiabatic boundary conditions are assumed from the surroundings.

According to the above assumption the governing conservation equations for mass, momentum and energy can be written as follow:

Mass conservation:

$$\frac{\partial u}{\partial x} + \frac{\partial v}{\partial y} = 0 \tag{1}$$

Momentum conservation:

$$\frac{\rho_{ncpcm}}{\varepsilon}\left(\frac{\partial u}{\partial t} + \frac{u}{\varepsilon}\frac{\partial u}{\partial x} + \frac{v}{\varepsilon}\frac{\partial u}{\partial y}\right) = -\frac{\partial p}{\partial x} + \frac{\mu_{ncpcm}}{\varepsilon}\left(\frac{\partial^2 u}{\partial x^2} + \frac{\partial^2 u}{\partial y^2}\right)$$
$$- A_m\frac{(1 - f_l)^2}{(f_l^3 - 0.001)}.u - \left(\frac{\mu_{ncpcm}}{K}u + \frac{C_F}{\sqrt{K}}\rho_{ncpcm}u\sqrt{u^2 + v^2}\right) \tag{2}$$

9

$$\frac{\rho_{ncpcm}}{\varepsilon}\left(\frac{\partial v}{\partial t}+\frac{u}{\varepsilon}\frac{\partial v}{\partial x}+\frac{v}{\varepsilon}\frac{\partial v}{\partial y}\right)=-\frac{\partial p}{\partial x}+\frac{\mu_{ncpcm}}{\varepsilon}\left(\frac{\partial^2 v}{\partial x^2}+\frac{\partial^2 v}{\partial y^2}\right)-(\rho\beta)_{ncpcm}g\varepsilon(T-T_{ref})$$
$$-A_m\frac{(1-f_l)^2}{(f_l^3-0.001)}.v-\left(\frac{\mu_{ncpcm}}{K}v+\frac{C_F}{\sqrt{K}}\rho_{ncpcm}v\sqrt{u^2+v^2}\right) \quad (3)$$

where, the ρ_{ncpcm}, μ_{ncpcm}, β_{ncpcm} are the density, dynamic viscosity, and thermal expansion coefficient of the NCPCM, respectively; p and g are the pressure and gravitational acceleration, respectively. A_m is the mush–zone constant which represents the damping of the velocity to zero during the solidification. The A_m constant does not affect the behaviour of melting time of PCM or NCPCM when MF is combined in the system. In present simulation, the value of A_m is set equal to the $A_m = 10^5$ [29, 30]. The small numerical value of 0.001 is used to prevent division by zero. The K is the permeability and C_F is the inertial coefficient of MF.

Since, the two models (i) local thermal equilibrium (LTE) and (ii) local thermal non–equilibrium (LTNE), are employed to solve the energy equation for PCM and NCPCM in presence of MF. However, the LTE model is used to solve the energy equation in present to save the computational resource without affecting the solution accuracy, in which the MF and PCM in each cell have the same temperature [29, 32]. Although, the LTNE model provide the more accurate solution compared with the LTE model because of considering the local convective heat transfer coefficient inside pores of porous between the metal–foam and PCM or NCPCM. Moreover, the difference between LTE and LTNE depends on the initial and boundary conditions which are more prominent while sensible heating mode rather than phase–change process due to having an most constant temperature. In addition, it is notable that, the LTNE model cannot be applied in 2D and axisymmetric models because of the generation of porous boundaries at the walls between the heat sink and PCM and limitation of coupled boundary condition for it in FLUENT software [31]. Thus, the energy equation with LTE is modelled as follows:

Energy conservation:

$$\overline{(\rho c_p)}\frac{\partial T}{\partial t}+(\rho c_p)_{ncpcm}\left(u\frac{\partial T}{\partial x}+v\frac{\partial T}{\partial y}\right)=k_{eff}\left(\frac{\partial^2 T}{\partial x^2}+\frac{\partial^2 T}{\partial y^2}\right)-\varepsilon\rho_{ncpcm}L_{ncpcm}\frac{\partial f_l}{\partial t} \quad (4)$$

The product $\overline{(\rho c_p)}$ is evaluated as the weighted average of the densities of MF and NCPCM as follows:

$$\overline{(\rho c_p)} = [1 - \varepsilon](\rho c_p)_{mf} + \varepsilon(\rho c_p)_{ncpcm} \tag{5}$$

where, $(\rho c_p)_{mf}$ and $(\rho c_p)_{ncpcm}$ are the volumetric heat capacities of MF and NCPCM, respectively. The L_{ncpcm} represent the latent–heat of fusion of NCPCM. The effective thermal conductivity (k_{eff}) introduced in LTE model, Eq. 4 is calculated as the volume average thermal conductivities of MF and NCPCM as follows:

$$k_{eff} = (1 - \varepsilon)k_{mf} + \varepsilon k_{ncpcm} \tag{6}$$

where, k_{mf} and k_{ncpcm} are thermal conductivity of MF and NCPCM, respectively. Additionally, f_l is the liquid–fraction during the phase–change in temperature interval of $T_s < T < T_l$ and it varies between 0 (solid) to 1 (liquid), which is defined as:

$$f_l = \frac{\Delta H_{ncpcm}}{L_{ncpcm}} = \begin{cases} 0 & \text{if} \quad T < T_s \\ \frac{T - T_s}{T_l - T_s} & \text{if} \quad T_s \leq T \leq T_l \\ 1 & \text{if} \quad T < T_l \end{cases} \tag{7}$$

where, ΔH_{ncpcm} is the fractional latent–heat of the NCPCM that gains during the phase–change process between 0 for solid and L_{ncpcm} for liquid during melting or releases during the solidification process. Thus, when all the NCPCM melts, ΔH_{ncpcm} is equal to the L_{ncpcm} and when the entire NCPCM is still solid, ΔH_{ncpcm} is equal to zero as follow:

$$\Delta H_{ncpcm} = \begin{cases} 0 & \text{if } T < T_m \\ f_l L_{ncpcm} & \text{if } T > T_m \end{cases} \tag{8}$$

The total enthalpy (H) of the NCPCM is the summation of sensible and latent–heat defined as:

$$H = h + \Delta H_{ncpcm} \tag{9}$$

where, h is the sensible enthalpy which is defined as follows:

$$h = h_{ref} + \int_{T_{ref}}^{T} c_{p_{ncpcm}} dT \tag{10}$$

Energy (heat sink):

$$(\rho c_p)_{HS} \left(\frac{\partial T}{\partial t} \right) = k_{HS} \left(\frac{\partial^2 T}{\partial x^2} + \frac{\partial^2 T}{\partial y^2} \right) \tag{11}$$

Energy (heat source):

$$(\rho c_p)_{hs} \left(\frac{\partial T}{\partial t} \right) = k_{hs} \left(\frac{\partial^2 T}{\partial x^2} + \frac{\partial^2 T}{\partial y^2} \right) + q^{'''} \tag{12}$$

where, $(\rho c_p)_{HS}$, k_{HS} $(\rho c_p)_{hs}$, and k_{hs} are the thermal capacitances and thermal conductivities of heat sink and heat source, respectively.

2.3. MF characterization

For laminar flow regime driven by pressure gradient, the permeability (K) is widely to develop the relationship between the pressure gradient and velocity. The permeability, K and inertial coefficient, C_F are determined using correlation proposed by Calmidi and Mahajan [33] as follows:

$$K = 0.00073(1 - \varepsilon)^{-0.0024} \left(\frac{d_l}{d_p} \right)^{-1.11} d_p^2 \tag{13}$$

and

$$C_F = 0.00212(1 - \varepsilon)^{-0.132} \left(\frac{d_l}{d_p} \right)^{-1.163} \tag{14}$$

The other basic parameters such as porosity (ε), ligament or cell diameter (d_l), pore diameter or pore size (d_p), and pore density (ω) are defined to describe the structure of MF. The porosity (ε) is the ratio of the pore volume to the MF total volume of pores and ligaments. The pore density (ω) is the number of pores per linear inch (PPI). The ligament diameter (d_l) can be calculated based on the pore diameter (d_p) as follows [33]:

$$\frac{d_l}{d_p} = 1.18 \sqrt{\frac{1 - \varepsilon}{3\pi}} \left(\frac{1}{1 - e^{-[(1-\varepsilon)/0.04]}} \right) \tag{15}$$

234 where, d_p is calculated as:

$$d_p = \frac{0.0254(m)}{\omega(PPI)} \tag{16}$$

235 *2.4. Thermophysical properties of NCPCM*

236 With the addition of Cu nanoparticles, the thermophysical properties of pure PCM are

237 changed by varying the volume fractions. All the effective properties of NCPCM are constant

238 except thermal conductivity and calculated based on the volume fraction of nanoparticles.

239 The effective density (ρ_{ncpcm}), specific heat capacity ($c_{p_{ncpcm}}$), latent–heat (L_{ncpcm}), and ther-

240 mal expansion coefficient (β_{ncpcm}) of the NCPCM can be calculated using simple theoretical

241 models of mixtures as follows [24–26, 28]:

$$\rho_{ncpcm} = \varphi\rho_{np} + (1 - \varphi)\rho_{pcm} \tag{17}$$

$$c_{p_{ncpcm}} = \frac{\varphi(\rho c_p)_{np} + (1 - \varphi)(\rho c_p)_{pcm}}{\rho_{ncpcm}} \tag{18}$$

$$L_{ncpcm} = \frac{(1 - \varphi)(\rho L)_{pcm}}{\rho_{ncpcm}} \tag{19}$$

$$\beta_{ncpcm} = \frac{\varphi(\rho\beta)_{np} + (1 - \varphi)(\rho\beta)_{pcm}}{\rho_{ncpcm}} \tag{20}$$

242 In above Eqs. 17–20, φ is the volume fraction of nanoparticles, the subscripts *ncpcm*,

243 *np* and *pcm* refer to the NCPCM, nanoparticles, and PCM, respectively. The effective

244 dynamic viscosity (μ_{ncpcm}) and thermal conductivity (k_{ncpcm}) of NCPCM are calculated

245 using modelled by the Vajjha et al.[34]:

$$\mu_{ncpcm} = 0.983e^{(12.959\varphi)}\mu_{pcm} \tag{21}$$

$$k_{ncpcm} = \frac{k_{np} + 2k_{pcm} - 2(k_{pcm} - k_{np})\varphi}{k_{np} + 2k_{pcm} + (k_{pcm} - k_{np})\varphi}k_{pcm} + 5 \times 10^4\beta_k\zeta\varphi\rho_{pcm}c_{p_{pcm}}\sqrt{\frac{BT}{\rho_{np}d_{np}}}f(T, \varphi) \tag{22}$$

246 where, B is Boltzmann constant which is equal to 1.381×10^{-23} J/K, $\beta_k = 8.4407(100\varphi)^{-1.07304}$,

13

and function $(f(T, \varphi))$ is defined as follows:

$$f(T, \varphi) = (2.8217 \times 10^{-2}\varphi + 3.917 \times 10^{-3})\frac{T}{T_{ref}} + (-3.0669 \times 10^{-2}\varphi - 3.91123 \times 10^{-3}) \quad (23)$$

where, T_{ref} is the reference temperature which is equal to 273.15 K. The first part of Eq. 23 relates with Maxwell model to determine the thermal conductivity of solid PCM while second part of Eq. 23 accounts the effects of Brownain motion of nanoparticles, nanoparticles size, volume fraction and temperature dependence. Additionally, ζ is a correction factor which comes in Brownian motion term, because there is no Brownian motion in solid–phase. Therefore, the value of ζ is defined as the same as for liquid–fraction, f_l [35]. The thermophysical properties of pure PCM (RT–35HC), Cu nanoparticles, all the MFs (Cu, Al and Ni) are summarized in Table 1.

2.5. Initial and boundary conditions

The initial and boundary conditions applied in current study are labelled in Fig. 1. The side walls of the heat sink are defined as an adiabatic boundary condition except the top surface which is undergoes the natural convection effect. Following are the initial and boundary conditions applied in this work to solve the governing equations as follows:

1. Initial conditions

   $t = 0$, $T = T_{ini} = 296.15$ K, $f_l = 0$

2. Boundary conditions

   - No–slip condition at walls: $u = v = 0$

   - Adiabatic walls:

     $-k \left.\frac{\partial T}{\partial x}\right|_{x=0,W} = 0$ Along vertical walls

     $-k \left.\frac{\partial T}{\partial y}\right|_{\substack{x=0-10,60-70 \\ y=0}} = 0$ At bottom surface

   - Natural convection:

     $-k\left.\frac{\partial T}{\partial y}\right|_{y=H} = h(T - T_\infty)$ At Top surface

   - Volumetric heat generation provided from heat source:

     $-k \left.\frac{\partial T}{\partial y}\right|_{\substack{x=10-60 \\ y=0-2}} = q'''$

14

2.6. Numerical methodology

The commercial package of CFD ANSYS–FLUENT 19.1 is used to solve the unsteady simulations. The governing equations of continuity, momentum and energy are solved are discretized by finite volume method (FVM) with double precision. The "melting/solidification" model in connection with local thermal equilibrium porous model is adopted to study the phase-change phenomenon of PCM or NCPCM. The melting/solidification model is based on the enthalpy-porosity method in which the solution is based on a fixed-gird. The governing equations are modified in such a manner that they are valid for both solid and liquid phases. The mush-zone where these both phases coexist is treated as "pseudo" porous medium where porosity behaves according to the liquid fraction. A User-defined function (UDF) is written in C++ language to account the temperature dependent k_{ncpcm} of NCPCM due to dispersion of Cu nanoparticles. The PRESSURE–BASED method is selected which is recommended for incompressible flow with high–order Quadratic Upstream Interpolation for Convective Kinematics (QUICK) differencing scheme presented by Leonard [37] to enhance the accuracy of the numerical method. The Semi-Implicit Pressure-Linked Equation (SIMPLE) algorithm was adopted for pressure–velocity coupling by Patanker [38]. The PRESTO (PREssure STaggering Option) scheme was adopted for pressure correction equation. The gravitational effect is also considered and second–order upwind difference scheme is selected to discretize convective terms in momentum and energy equations. The under-relaxation factors for pressure, velocity, energy and liquid-fraction are set to 0.3, 0.3, 0.8 and 0.5, respectively. The convergence criteria are set to 10^{-4}, 10^{-6} and 10^{-8} for continuity, momentum and energy equations, respectively.

The grid independence test is also carried out using different gird size of 43753, 48305, 54087 and 60796 to avoid its effects on numerical accuracy. The results of melting time and total energy of PCM are summarized in Table 2. The maximum deviation in melting time and total energy is obtained of 0.38% and 0.06% between the elements size of 48305 and 54087, respectively. Thus, the grid with the size of 54087 elements is selected for further simulation. Three different time-steps of 0.05, 0.1 and 0.2 s are varied for mesh size of 54087 elements and no significance variation is observed. The reason is that PCM upfront velocity and thermal front movement are low, reflecting a low Peclet number and Courant number situation. Therefore, the mesh-size and time-step are 54096 elements and 0.1s, respectively, considered are set in current study.

15

2.7. Performance evaluation parameters

To estimate the thermal performance of pure PCM, NCPCM, MF+PCM and NCPCM+MF based heat sink, four different performance evaluation parameters such as heat storage capacity (Q), heat storage density (q), rate of heat transfer ($\dot{Q}$), and rate of heat transfer density ($\dot{q}$) along with the total melting time (t_{melt}). The total Q is defined as the total thermal energy storage capacity during the pre–sensible heating, latent–heat of fusion, and post–sensible heating of pure PCM or NCPCM. Whereas, q indicates the total thermal energy storage capacity per unit mass of the pure PCM or NCPCM. Since, the pre–sensible heating and latent–heat are the most significant parameters to determine the Q of pure PCM, NCPCM, MF+PCM and NCPCM+MF based heat sink whiling charging mode. Therefore, Q and q can be defined by Eqs. 24 and 25, respectively, as follows [39]:

$$Q = m_{mf} \int c_{p_{mf}} dT + m_{ncpcm} \left(\int_{solid} c_{p_{ncpcm}} dT + \lambda L_{ncpcm} + \int_{liquid} c_{p_{ncpcm}} dT \right)$$
$$\approx m_{ncpcm}[c_{p_{ncpcm}}(T_m - T_i) + f_l L_{ncpcm}] \quad (24)$$

and

$$q = \frac{Q}{m_t} = \frac{m_{mf} \int c_{p_{mf}} dT + m_{ncpcm} \left(\int_{solid} c_{p_{ncpcm}} dT + f_l L_{ncpcm} + \int_{liquid} c_{p_{ncpcm}} dT \right)}{m_{mf} + m_{ncpcm}}$$
$$\approx \frac{m_{ncpcm}[c_{p_{ncpcm}}(T_m - T_i) + f_l L_{ncpcm}]}{m_{mf} + m_{ncpcm}} \quad (25)$$

Since, the Q and q can only evaluate the storage capacity of pure PCM, NCPCM, MF+PCM and NCPCM+MF based heat sink relative to the mass of PCM or NCPCM. However, there is no relationship of total t_{melt} of PCM or NCPCM with Q and q. Thus, the overall thermal performance of heat sink cannot be evaluate only with Q and q. Therefore, the effect of t_{melt}, m_{mf}, m_{ncpcm}, and Q are combined together to define the rate of heat transfer ($\dot{Q}$) and rate of heat transfer density ($\dot{q}$). The $\dot{Q}$ indicates the total thermal energy storage capacity per unit melting time and $\dot{q}$ is defined as total thermal energy storage capacity per unit melting time and per unit mass of MF ad PCM or NCPCM, by Eqs. 26 and 27, respectively, as follows:

$$\dot{Q} = \frac{Q}{t_{melt}} = \frac{m_{mf}\int c_{p_{mf}}dT + m_{ncpcm}\left(\int_{solid} c_{p_{ncpcm}}dT + f_l L_{ncpcm} + \int_{liquid} c_{p_{ncpcm}}dT\right)}{t_{melt}}$$

$$\approx \frac{m_{ncpcm}[c_{p_{ncpcm}}(T_m - T_i) + f_l L_{ncpcm}]}{t_{melt}} \quad (26)$$

and

$$\dot{q} = \frac{Q}{t_{melt}.m_t} = \frac{m_{mf}\int c_{p_{mf}}dT + m_{ncpcm}\left(\int_{solid} c_{p_{ncpcm}}dT + f_l L_{ncpcm} + \int_{liquid} c_{p_{ncpcm}}dT\right)}{t_{melt}.m_{ncpcm}}$$

$$\approx \frac{m_{ncpcm}[c_{p_{ncpcm}}(T_m - T_i) + f_l L_{ncpcm}]}{t_{melt}(m_{mf} + m_{ncpcm})} \quad (27)$$

3. Model validation

3.1. Experimental validation with PCM based heat sink

The current model is validated with experimental results of a no fin heat sink filled with PCM having the dimension of similar dimensions used in Ashraf et al. [5]. The RT–35HC was used as a PCM having melting temperature of 35 °C at a input power level of 5W. The results of average temperature of heat sink was compared of both numerical and experimental cases, as shown in Fig. 3a. The results of both numerical and experimental results showed a good agreement and revealed that the present numerical model can be used for further simulations.

3.2. Experimental and numerical validation MF/PCM based thermal energy storage

A comprehensive validation is carried with the previous experimental and numerical studies reported by Zhao et al. [16] and Tian and Zhao [17], respectively, and numerical study by Liu et al. [40] by using both LTE and LTNE models of MF+PCM system. The 2D system of MF+PCM is adopted for validation proposed in experimental and numerical results of Zhao et al. [16] and Tian and Zhao [17] and as well as Liu et al. [40]. A rectangular geometry having the dimensions of 200×50 mm^2 is selected and a constant heat flux of 1600 W/m^2 is provided at the bottom. The RT–58 is used as a PCM and Cu MF having 95% porosity and 10 PPI. Natural convection effects are considered at the side and top walls as considered in Refs. [16, 17] and [40] to get the more better results. The result of temperature variations are presented at a height of 8 mm in comparison with the Zhao et al. [16] and

17

Tian and Zhao [17], as shown in Fig. 3b. A excellent agreement can be seen between the LTNE model of present study with experimental and numerical results with Refs. [16, 17] and numerical results of Ref. [40]. The results of LTE model also show a good agreement with LTE model results reported by Liu et al. [40]. The variations in results of numerical and experimental studies reported in Zhao et al. [16] and Tian and Zhao [17], respectively, are because of considering a constant melting temperature in numerical study, as reported in Liu et al. [40]. Therefore, in present study and the study reported by Liu et al. [40] use the different solidus (T_s) and liquidus (T_l) temperatures for the simulations. The maximum deviation of ±4.2 °C is obtained between the current study results and experimental results of Zhao et al. [16]. In addition, it is always difficult to justify the discrepancy in results, shown in Fig. 3b, because the data is taken out from the experimental and numerical results of electronic copies of Refs [16, 17, 40]. Although, the LTNE model can predict the T_{HS} and f_l more accurately compared to the LTE model. However, due the to higher computational cost of LTNE model in porous–PCM medium, especially in 3D solid–liquid cases, LTE model is employed for further analysis. It has been revealed in previous studies, the difference between LTE and LTNE models is very small due to the primary domination of heat conduction rather than the natural heat convection effect [41].

4. Results and discussion

4.1. Effect of MF materials

The average heat sink temperature (T_{HS}) and melt–fraction (f_l) variations for PCM, Cu, Al and Ni MF+PCM cases are shown in Fig. 4a. The uniform and non–uniform melting of PCM can been seen clearly for PCM and MF+PCM embedded heat sinks cases. At a constant input power level, the transient variation of T$_{HS}$ for each case shows that MF+PCM embedded heat sinks have the significant reduction in heat sink temperature, as shown in Fig. 4a. The reduction in T_{HS} is due to uniform heat transfer from the heat sink base towards the ambient due to conjugate heat transfer mode. This reveals that a heat sink embedded with MF+PCM has the better heat transfer performance. Thus effective cooling performance is achieved compared to a heat sink of pure PCM filled. A closer look of temperature variation between the different materials of MF reveals that Cu MF+PCM heat sink shows the better reduction in T_{HS} compared to the Al and Ni MF+PCM embedded heat sinks. The reduction in heat sink temperature by Cu MF heat sink is because of the higher thermal conductivity of Cu, followed by Al and Ni. The variations in f_l of all cases,

18
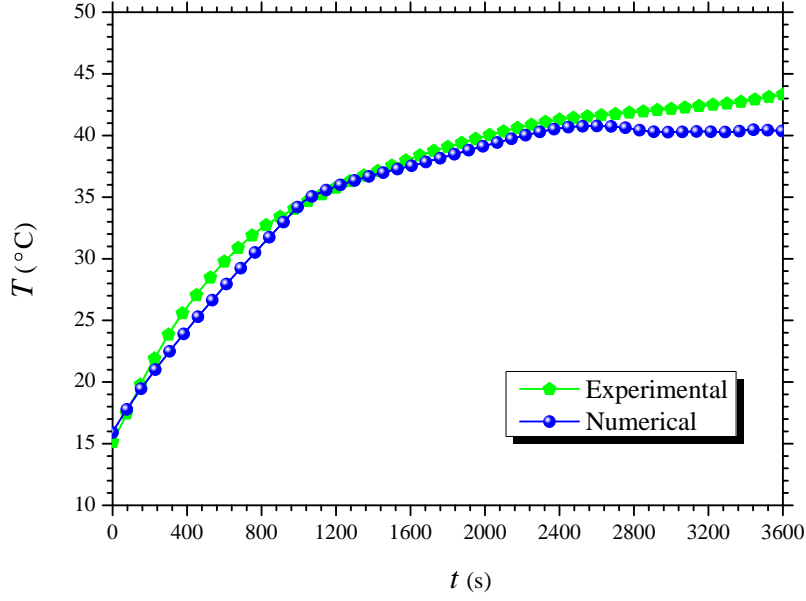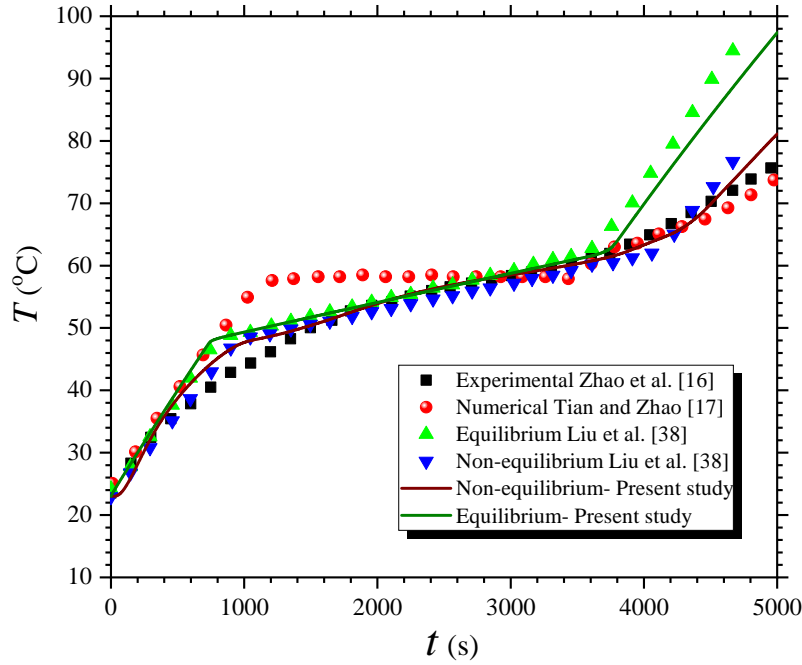
Figure 3: *Validation of present simulation (a) with experimental results based on PCM case and (b) experimental results by Zhao et al. [16] and Tian and Zhao [17], and numerical results by Liu et al. [40] with MF case.*

shown in Fig. 4a, reveals that the higher rate of f_l is obtained for the MF cases compared to the pure PCM case because of the higher heat transfer area by MF+PCM which strengthen the conduction heat transfer. The melting rate is different between the PCM and MF+PCM cases. The variation in f_l of MF embedded heat sinks is slightly varying and the highest f_l is obtained by Cu MF heat sink, followed by Al and Ni MF heat sinks. This trend is expected since Cu has the higher thermal conductivity compared to Al and Ni. The evolution of t_{melt},

19

Q and $\dot{Q}$ of all cases is shown in Fig. 4b. It can be seen that the t_{melt} of PCM is decreased by embedding the MF+PCM and lower time of 44.17 min is obtained with Cu MF+PCM compared to PCM, Al and Ni MF+PCM filled heat sink cases by obtaining 53.42, 44.92, and 47.08 mins, respectively. The reduction in t_{melt} is obtained of -17.32%, -15.91% and -11.86% for Cu, Al and Ni MF+PCM cases compared to the pure PCM case. The similar trend is obtained in Q for pure PCM and MF+PCM cases. The Q of 279.78, 266.15, 266.27 and 270.76 kJ are obtained for PCM, Cu, Al and Ni MF+PCM heat sinks, respectively. The reductions in Q due to embedding the MFs are achieved of -4.87%, -4.83% and -3.22% for Cu, Al and Ni MF+PCM heat sinks, respectively. However, the enhancement in $\dot{Q}$ is obtained with MF+PCM compared to the pure PCM based heat sink. The $\dot{Q}$ for pure PCM, Cu, Al and Ni MF+PCM heat sinks is obtained of 80.28, 86.84, 86.31 and 84.30 W, respectively. It can be revealed that highest enhancement of 8.16% in $\dot{Q}$ is obtained with Cu MF+PCM compared to the Al and Ni MF+PCM of 7.51% and 5.01%, respectively, compared to the pure PCM filled heat sink, because of the higher thermal conductivity. Thus, it can be suggested that a PCM filled heat sink with Cu MF+PCM shows the better thermal cooling performance. Since, the Fig. 4 presents thermal cooling performance in terms of T_{HS}, f_l, t_{melt}, Q and $\dot{Q}$, however the further comparison of melting phenomenon of pure PCM and all MF+PCM embedded heat sinks is shown in Fig. 5. The f_l contours are presented at different flow times of 900, 1500, 2100, 2700 and 3300 s. It can be seen clearly that by using MF+PCM, the melting pattern of PCM melting changes significantly. In addition, the uniform and faster melting of PCM is obtained with the case of MF+PCM embedded heat sinks especially in case of Cu MF+PCM followed by Al and Ni MF+PCM heat sinks. Initially, at 900 s, the layers of solid–liquid interface (i.e. heat transfer area) can been seen clearly through blue and red colours, respectively, for a PCM heat sink case. Whereas a uniform melting patterns can be seen with MF+PCM heat sinks by showing no visible solid–liquid interface. With the increase of melting time, the gradually solid–liquid interface can be seen showing the effect of buoyancy and gravitational forces. A uniform melting is observed in case of MF heat sinks due the conduction and natural convection heating modes. At 3300 s, the complete melting of PCM is observed in case of MF+PCM whereas there is still small tiny portion of solid PCM, which shows that the addition of MFs with PCM improves the heat transfer rate and melting process uniformly.
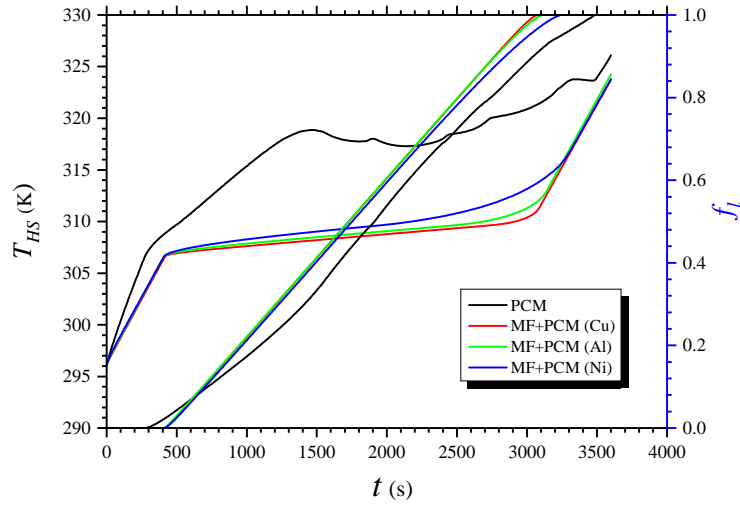
(a)
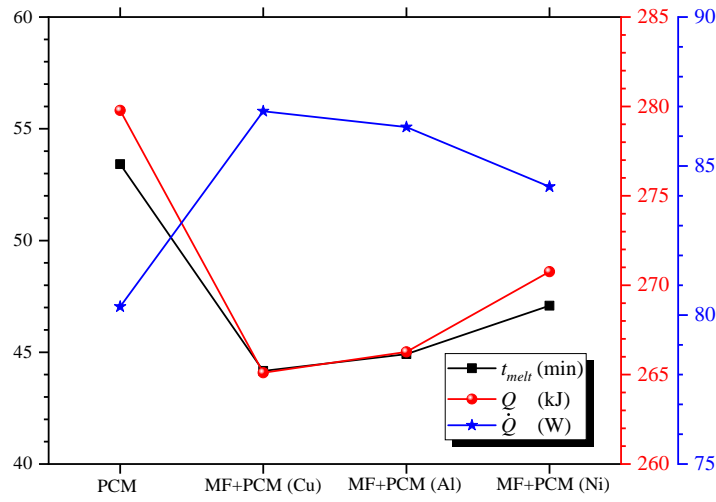
(b)

Figure 4: *Effect of different MF materials: (a) T_{HS} and f_l, and (b) t_{melt}, Q and $\dot{Q}$.*

4.2. Effect of power levels

Fig. 6 presents the effect of different power levels of a Cu MF+PCM embedded heat sink. The T_{HS} and f_l results are presented in Fig. 6a. Whereas, the comparison of t_{melt} and $\dot{Q}$ at different power levels are presented in Fig. 6b. It is can be seen that latent–heating phase duration of PCM is reduced and T_{HS} is increased as the input power level increase, as expected. In addition at lower input power of 4 W, there is no phase changing occurred even after 3600 s and supplied heat is absorbed by the PCM due to its higher latent–heat enthalpy. The maximum T_{HS} and f_l of 309.62 °C and 0.941 are obtained at lower power level of 4 W. The comparison of t_{melt} and $\dot{Q}$ of Cu MF+PCM embedded heat sink shows that with the increase of power level, the t_{melt} of PCM is decreased whereas $\dot{Q}$ increases, as shown in Fig. 6b. The t_{melt} of PCM is obtained of 44.17, 36.83, 31.58, and 27.75 mins for 5, 6, 7, and 8 W, respectively. Similarly, the $\dot{Q}$ is obtained of 86.84, 104.34, 121.81, and 139.19

21

(a) 900 s, PCM (b) 900 s, Cu$_{mf}$+PCM (c) 900 s, Al$_{mf}$+PCM (d) 900 s, Ni$_{mf}$+PCM

(e) 1500 s, PCM (f) 1500 s, Cu$_{mf}$+PCM (g) 1500 s, Al$_{mf}$+PCM (h) 1500 s, Ni$_{mf}$+PCM

(i) 2100 s, PCM (j) 2100 s, Cu$_{mf}$+PCM (k) 2100 s, Al$_{mf}$+PCM (l) 2100 s, Ni$_{mf}$+PCM

(m) 2700 s, PCM (n) 2700 s, Cu$_{mf}$+PCM (o) 2700 s, Al$_{mf}$+PCM (p) 2700 s, Ni$_{mf}$+PCM

(q) 3300 s, PCM (r) 3300 s, Cu$_{mf}$+PCM (s) 3300 s, Al$_{mf}$+PCM (t) 3300 s, Ni$_{mf}$+PCM
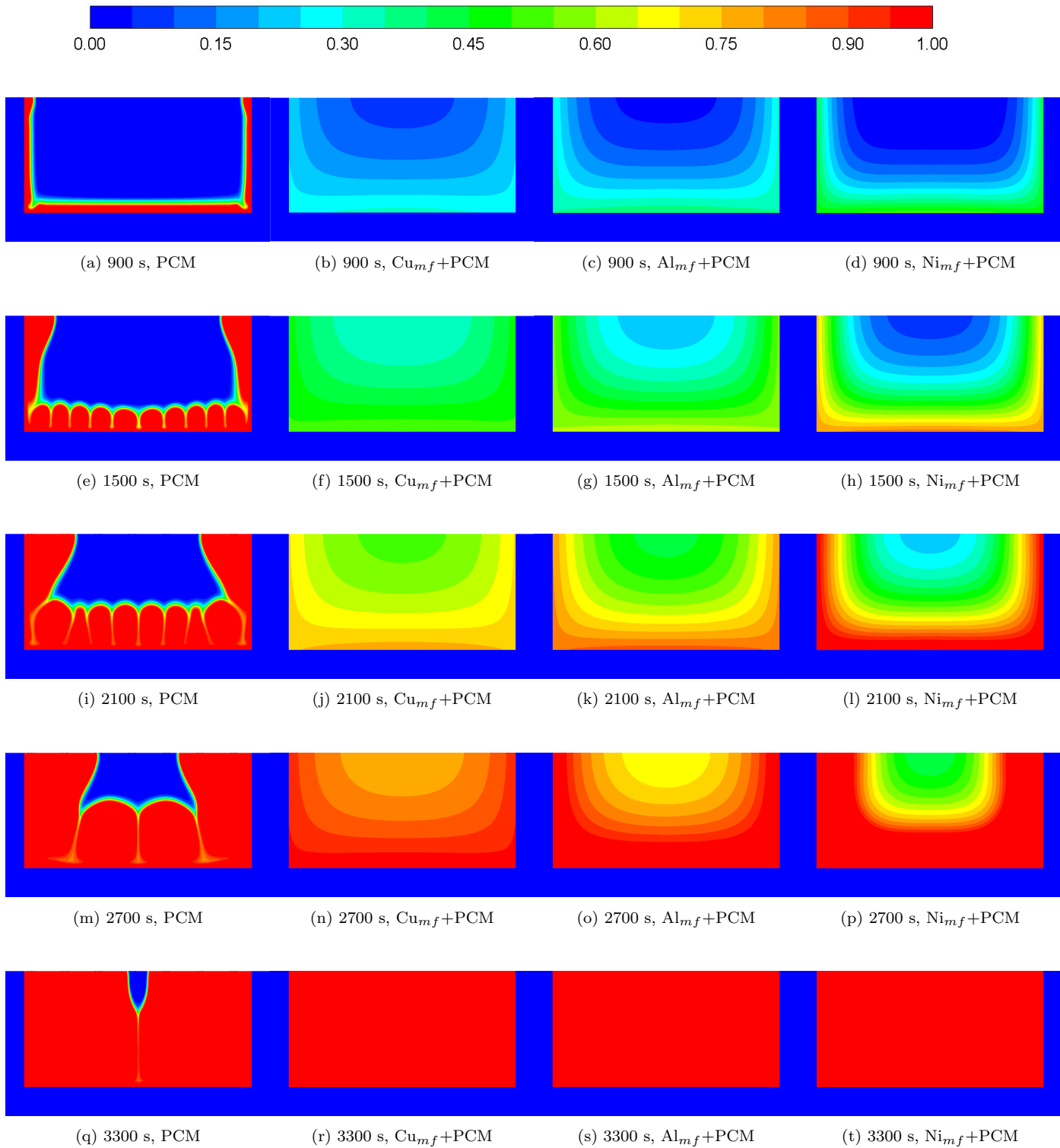
Figure 5: *Variation of f_l at various t of PCM, Cu, Al and Ni MF+PCM embedded heat sinks.*

W for 5, 6, 7, and 8 W, respectively. The higher $\dot{Q}$ is because of the lower t_{melt} of PCM filled in MF heat sink. Furthermore, it can be suggested that at lower power level, the T_{HS} does not rise enough to melt the PCM. Therefore, a MF+PCM embedded heat sink has less advantage for passive thermal management of electronic devices at lower power level.
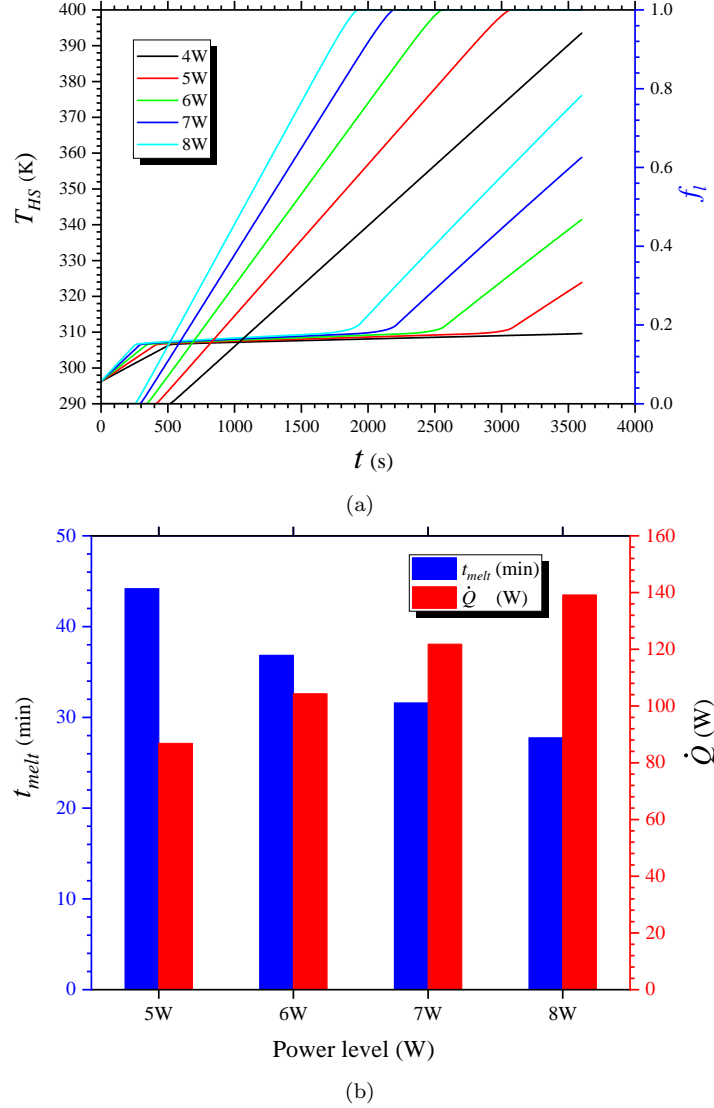
Figure 6: *Effect of different power levels of MF+PCM filled heat sink: (a) T_{HS} and f_l, and (b) t_{melt} and $\dot{Q}$.*

4.3. Effect of PPI

Fig. 7 shows the effect of changing the PPI or pore density of MF embedded in a PCM filled heat sink. The five different values of 10, 20, 30, 40 and 50 PPI are investigated of Cu MF+PCM heat sink a constant porosity of 95% and input power level of 5 W. A slight variation in t_{melt} of PCM is obtained by changing the PPI of MF. The t_{melt} of PCM is obtained of 44.17, 44.08, 44.0, 43.92, and 43.83 mins for 10, 20, 30, 40 and 50 PPI, respectively. It

can be revealed that a small variation in t_{melt} and temperature distribution is achieved by changing the PPI of MF under local thermal equilibrium heat transfer conditions. Furthermore, a closer look of t_{melt} result reveals that a MF with lower PPI enhances the t_{melt} of MF+PCM filled heat sink resulting in reduces the base temperature of the heat sink. The higher number of PPI means the unit cell is divided into higher number of small pore which reduce the effect of low thermal conductivity of the PCM. In addition, a higher value of PPI contains a smaller size of a pore which possesses the higher surface area per unit volume. Thus, higher heat transfer rate exists between the PCM and MF ultimately reduces the t_{melt} of the PCM. Contrarily, the higher PPI suppresses the natural convection effect of PCM melting with the MF because of the high thermal resistance in the PCM flow direction. Thus, the influence of PPI is negligible for a MF+PCM embedded heat sink under local thermal equilibrium heat generation conditions which has also been reported in literature [40, 42]. As shown in Fig. 7 that negligible effect of PPI is achieved on the variation of f_l. The higher f_l is obtained by increasing the PPI from 10 to 50.
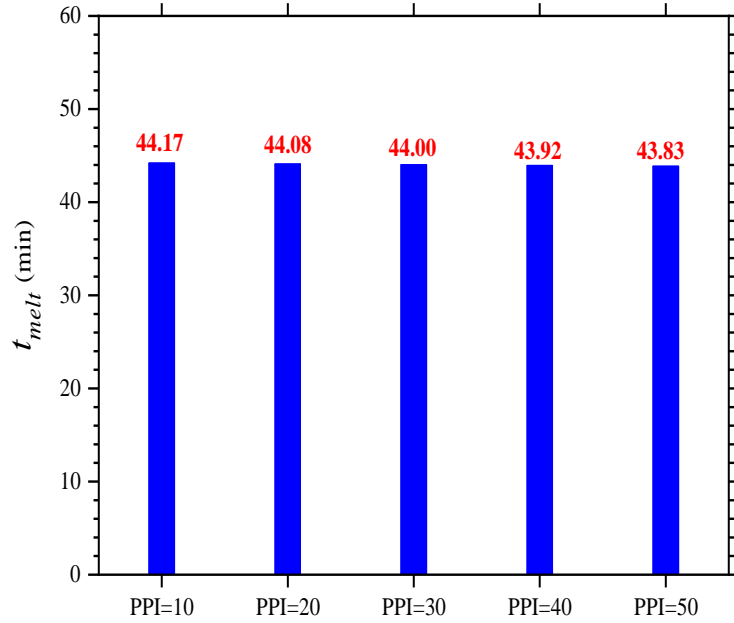
Figure 7: *Effect of different PPI: comparison of PCM t_{melt}.*

4.4. Effect of Porosities

Fig. 8 illustrates the effect of different porosities (95%, 90%, and 80%) of Cu MF+PCM embedded heat sink compared with the pure PCM filled heat sink with 10 PPI at 5W. The result of T_{HS} and PCM f_l as a function of time are presented in Fig. 8a for MF+PCM and PCM cases. It can be seen clearly that T_{HS} reduces significantly by embedding the MF

24

inside the heat sink. In addition, a close look of the T_{HS} and f_l results of the porosities 95%, 90%, and 80% show that a Cu MF+PCM based heat sink of 95% porosity has lower T_{HS} and f_l. The minimum T_{HS} of 323.09 °C is obtained with 95% MF+PCM heat sink compared with 90%, 80% and pure PCM heat sink cases. More further, a lower f_l is obtain with 95% MF+PCM heat sink compared with 90% and 80% MF+PCM cases. Since, the complete meting of PCM occurs after 3065 s. By increasing the porosity of MF, as a result reduced the amount of higher thermal conductivity MF inside the heat sink, thus higher PCM melting time is achieved due to lower rate of heat transfer, as expected.

Fig. 8b shows the results of t_{melt}, the amount of Q and $\dot{Q}$ of all cases of PCM and MF+PCM filled heat sinks. The t_{melt} and Q are reduced with the reduction of porosity since higher amount of MF inside the heat sink exhibits the higher effective thermal conductivity of the PCM result in increases the heat transfer rate. The reduction in t_{melt} and Q are obtained of -17.32% and -4.87%, -20.28% and -5.44%, and -22.93% and -5.46% for 95%, 90%, and 80% MF+PCM, respectively, compared with PCM filled heat sinks. Whereas, in comparison with PCM filled heat sink, the $\dot{Q}$ is increased of 8.16%, 10.77% and 13.22% with 95%, 90%, and 80% MF+PCM cases, respectively. Therefore, it can be suggested that a heat sink with constant mass of PCM, the higher porosity of 95% is favourable for passive thermal cooling of electronics, since it prolongs the PCM t_{melt} duration and lower the T_{HS}.

4.5. Effect of NCPCM

Fig. 9 reveals the effect of nanoparticles dispersion in PCM filled heat sink by varying the loading contents of 1%, 3% and 5%. The addition of higher thermal conductivity nanoparticles improve the thermal conductivity of pure PCM on the cost of decreasing the latent–heat of fusion and specific heat capacity which is not preferable for passive cooling of electronic components. The results of T_{HS} and f_l, as shown in Fig. 9a, reveal that T_{HS} is decreased initially but reaches higher as the volume fraction of nanoparticles increases. Further, the higher f_l is obtained with the increase of nanoparticles loadings which improve the PCM melting rate. Since the amount of PCM increases with the increase of nanoparticles loadings, the time of complete PCM melting is almost constant. The t_{melt} of PCM is obtained of 52.75, 52.45 and 52.17 mins for 1%, 3% and 5% volume factions of Cu nanoparticles, respectively, as shown in Fig. 9b. The t_{melt} is reduced of -1.25%, -1.87%, and -2.34% by 1%, 3% and 5% concentrated NCPCM heat sink, respectively, compared with PCM filled heat sink. Similarly, the results of Q and $\dot{Q}$ are almost negligible. The Q and $\dot{Q}$ are

25
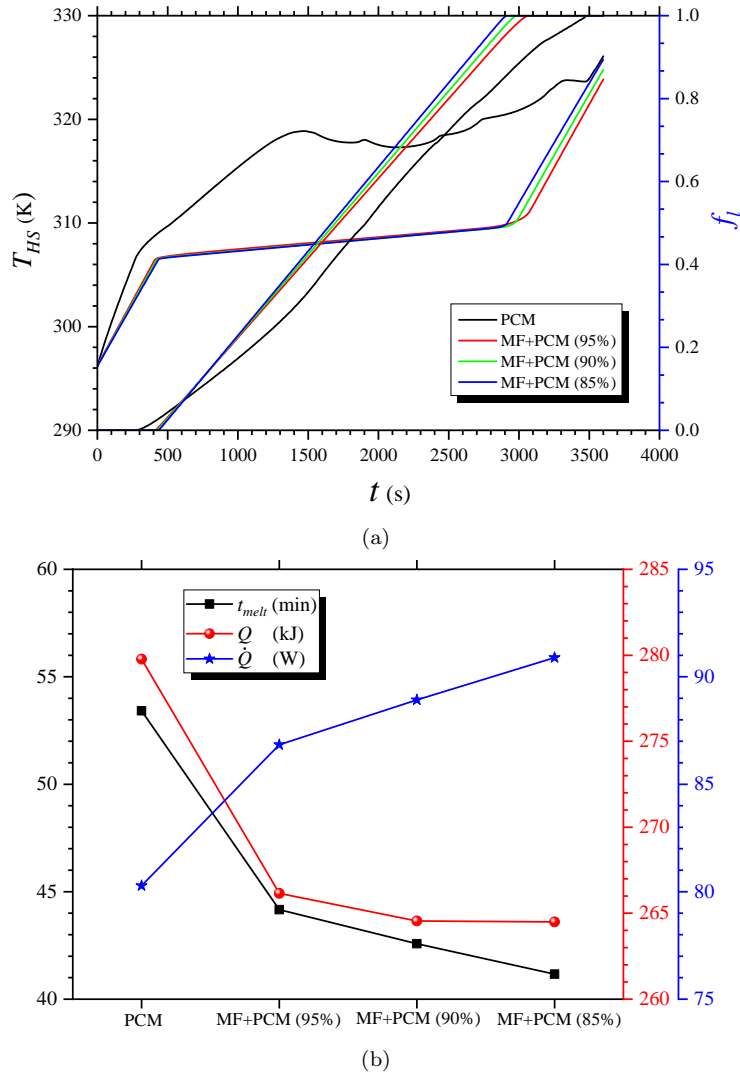
Figure 8: *Effect of different porosities: (a) T_{HS} and f_l, (b) t_{melt}, Q and $\dot{Q}$.*

increased initially at 1% of Cu nanoparticles concentration, however, these are decreased for later on 3% and 5% NCPCM cases which is due to the increase of PCM mass by adding the nanoparticles. Since, the system has a close boundary so the heat sink volume is constant however, by the addition of nanoparticles the thermophysical properties such as density, latent–heat of fusion, thermal expansion coefficient, specific heat capacity, viscosity and volumetric heat capacity of PCM are changed which also effect the thermal performance of heat sink. The $\dot{Q}$ is enhanced by 1.35%, 0.76%, and 0.19% by adding 1%, 3% and 5% volume concentration of Cu nanoparticles, respectively, compared with the PCM filled heat sink case. Similarly, the variations in $\dot{Q}$ are obtained of 0.34%, −0.69%, and −1.68% for 1%, 3% and 5% NCPCM cases, respectively, compared with PCM filled heat sink. It can been reveal that $\dot{Q}$ and best Q are obtain at 1% of Cu nanoparticles concentration. Therefore, it is recommended that by adding 1% loading of nanoparticles has the optimum results in

terms of thermal cooling performance because the higher concentrations can lead toward the agglomeration and sedimentation of nanoparticles in real time system. Additionally, these are also reduced the latent–heat fusion and increase t_{melt} of PCM. A rapid decreasing trend can observed in results of q and $\dot{q}$ because of increase of the PCM mass with the increase of Cu nanoparticles concentrations, as shown in Fig. 9b. By adding the 1%, 3% and 5% loadings of Cu nanoparticles the q is decreased of -8.63%, -23.27%, and -34.04%, respectively, compared with PCM filled heat sink case. In similar manner, the $\dot{q}$ for NCPCM filled heat sinks is reduced by -7.70%, -22.16%, and -32.79%, respectively, compared with PCM filled heat sink.

For better understanding the effect of NCPCM heat sinks of different volume fractions, Figs. 10a and 10b illustrate the results of k_{eff} and k_{eff} enhancement, respectively, for PCM and NCPCM filled heat sinks. It can be seen that k_{eff} increases with the increase of Cu nanoparticles concentration with respect to time. More further, it has been reported that k_{eff} also increases and decreases with respect to temperature during melting and solidification processes, respectively, with the increase of nanoparticles loading by using Equation 22 [28]. After 3600 s, the maximum enhancement in k_{eff} are obtained of 17.99%, 24.33%, and 31.50% for 1%, 3% and 5% loadings of Cu nanoparticles.

Further, the distribution of T_{HS} at the surface of heat sink in vertical direction is shown in Fig. 11 by representing the isotherm contours at different time intervals for different φ of Cu nanoparticles. The T_{HS} is increased gradually with the increase of operating time and φ during the melting process. Initially, at the 1200 s, the lower to higher variation in T_{HS} can be seen for all cases of PCM and NCPCM filled heat sinks over the surface because of the conduction and natural convection modes. A clear observation of conduction heat transfer is reflected at the boundaries of PCM and heat sink due to the temperature gradient. During the heating process, a uniform the distribution of T_{HS} isotherms is seen between the solid– liquid interfaces of both PCM and NCPCM filled heat sinks which that the conduction heat transfer mode is more dominant than convection mode. With the increase of time from 1800 to 3000 s, the both conduction and natural convection heat transfer modes are observed from the isotherms for all heat sink cases by seeing the deformation in PCM shape, which shows the initiating of natural convection inside the heat sink. In addition, the circulating pattern of isotherms are observed at the bottom of the heat sink because of the buoyancy effects and gravity force. The more dominant convection patterns of isotherms are obtained with the increase of time, developed by the temperature gradient, because of the growing role of

convection heat transfer in melt zone.

The further visualization of melting phenomenon of PCM and NCPCM filled heat sink cases is illustrated using f_l contours presented in Fig. 12. Initially, at 1200 s, there are clear zones of solid and liquid PCM representing by blue and red colours, respectively, and layers of PCM melting can be observed at the bottom and sides walls for all heat sink cases. With the increase of melting time, at 1800 and 2400 s, the clear observation of circulating patterns of liquid PCM is found at the bottom of the heat sink due the effect of buoyancy and gravity forces. Since, the addition of nanoparticles enhance the thermal conductivity of NCPCM as the well as the viscosity of NCPCM which enhance the heat transfer rate and also affects the melt movement of PCM. Therefore, conduction heat transfer mode dominates over convection mode. In addition, the significance of natural convection is noticeable by appearing the more deformation and size of rotating circles of melted PCM during melting process of NCPCM. Moreover, a regular decrease in circulating patterns is observed with the increase of nanoparticles volume fraction. A closer look reveals that relative cold PCM moves downward from solid–liquid interface because of gravitational effect which improves the complete melting of PCM. This movement of melted PCM enhances the rate of PCM melting at the bottom half of the heat sink compared to the upper half. Later on during the melting process, at 3000 s, the higher rate of f_l of NCPCM is obtained in most of the part of heat sink domain which shows the dominant contribution of natural convection heat transfer because of the influence of buoyancy effects. There is still movement of cold or relative less melted PCM towards the bottom because of gravity effects. At 3600s, the complete melting of NCPCM is obtained for 1%, 3%, and 5% φ because of conduction and natural convection contribution. Since, the addition of nanoparticles improves the thermal conductivity of PCM, thus, it improves the conductive heat transfer rate within the PCM and faster melting is achieved.

4.6. Effect of different nanoparticles concentrations with constant MF

Fig. 13 presents the effect of varying Cu nanoparticles volume concentrations in presence of MF+PCM filled heat sink. The constant porosity and PPI of 95% and 10 are selected, respectively, and three different volume fractions of 1%, 3% and 5% of Cu nanoparticles are investigated individually. Since it has been explored that the MF having 95% and 10 porosity and PPI, respectively, has the best thermal cooling performance. Thus, effect of nanoparticles concentrations are investigated further with MF+PCM embedded heat sink.

28
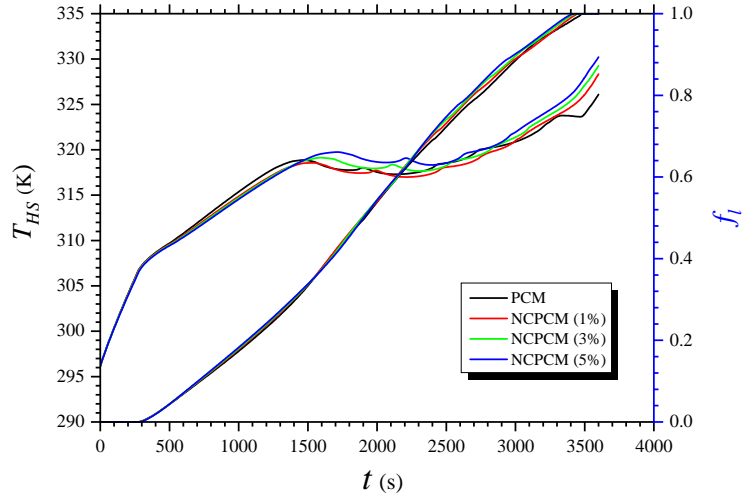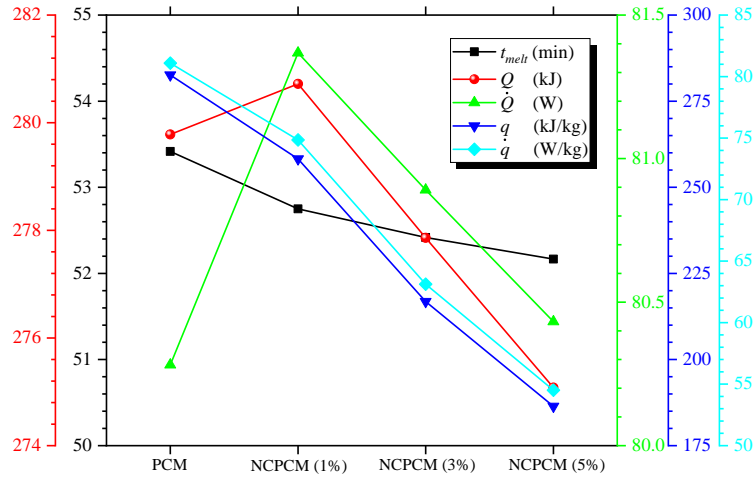
Figure 9: *Effect of PCM and NCPCMs filled heat sink: comparison of (a) T_{HS} and f_l, (b) t_{melt}, Q, $\dot{Q}$, q and $\dot{q}$.*

Fig. 13a shows the results of T_{HS} and f_l for PCM, MF+PCM and MF+NCPCM heat sink cases at a constant input power level of 5 W. The lower T_{HS} and higher f_l are obtained for both MF+PCM and MF+NCPCM heat sink cases. Furthermore, a closer look reveals that MF+NCPCM heat sink has the higher f_l and less latent–heat phase–change duration result in increases the T_{HS} after complete melting of PCM. The melting durations of PCM are obtained of 53.42, 44.17, 43.75, 42.92, and 42.08 mins for the case of PCM, MF+PCM, MF+NCPCM (1%), MF+NCPCM (3%), and MF+NCPCM (5%), respectively, as shown in Fig. 13b. A reduction in PCM t_{melt} was obtained of -17.32%, -18.10%, -19.66%, and -21.22% for MF+PCM, MF+NCPCM (1%), MF+NCPCM (3%), and MF+NCPCM (5%), respectively, compared with PCM filled heat sink. Since, both MF and nanoparticles have the higher thermal conductivity which results in enhance the heat transfer rate within PCM and reduced the t_{melt}. Similarly, a decreasing trend in results of Q are obtained and
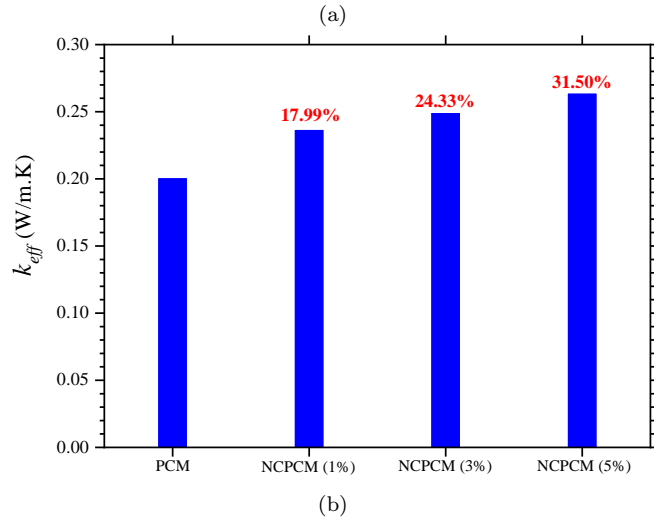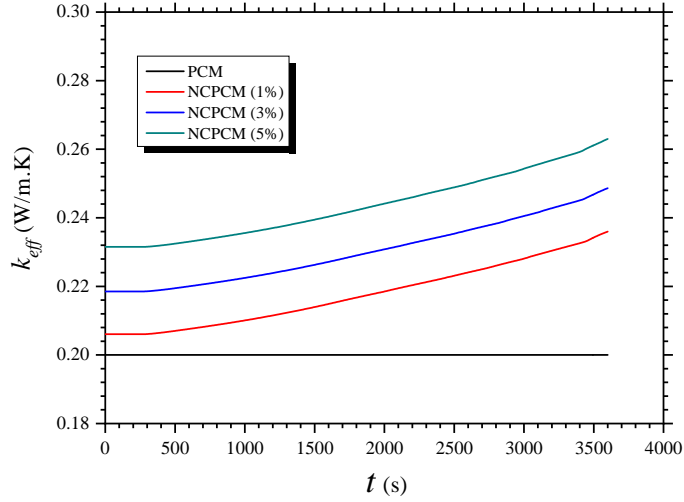
Figure 10: *Results of (a) k_{eff} (b) k_{eff} enhancement of NCPCMs.*

a reduction of -4.87%, -5.68%, -7.19%, and -8.70% for MF+PCM, MF+NCPCM (1%), MF+NCPCM (3%), and MF+NCPCM (5%), respectively, compared with PCM filled heat sink. It can be seen that a slight variation in $\dot{Q}$ of MF+PCM and MF+NCPCM heat sinks cases. The $\dot{Q}$ sharply increases by adding the MF however, by adding the Cu nanoparticles of 1%, 3%, and 5% it is slightly decreased which is less significant in overall thermal performance. The enhancement in $\dot{Q}$ is obtained of 8.16%, 8.12%, 7.99%, and 7.86% for MF+PCM, MF+NCPCM (1%), MF+NCPCM (3%), and MF+NCPCM (5%), respectively, compared with PCM filled heat sink. It can be seen from Fig. 13b that sharp decreasing trend is obtained in results of q and $\dot{q}$ for the case of MF+NCPCM heat sinks which is due to increase of the total mass of the PCM by adding the different concentrations of nanoparticles. The q is reduced by -4.87%, -14.11%, -28.30%, and -38.75% for MF+PCM, MF+NCPCM (1%), MF+NCPCM (3%), and MF+NCPCM (5%), respectively, compared with PCM filled heat sink. The result of $\dot{q}$ presents that $\dot{q}$ increases by 8.16% adding the MF

30

Static Temperature (k)

| 300.0 | 302.3 | 304.5 | 306.8 | 309.0 | 311.3 | 313.5 | 315.8 | 318.0 | 320.3 | 322.5 |

(a) 1200 s, PCM (b) 1800 s, PCM (c) 2400 s, PCM (d) 3000 s, PCM

(e) 1200 s, NCPCM (1%) (f) 1800 s, NCPCM (1%) (g) 2400 s, NCPCM (1%) (h) 3000 s, NCPCM (1%)

(i) 1200 s, NCPCM (3%) (j) 1800 s, NCPCM (3%) (k) 2400 s, NCPCM (3%) (l) 3000 s, NCPCM (3%)

(m) 1200 s, NCPCM (5%) (n) 1800 s, NCPCM (5%) (o) 2400 s, NCPCM (5%) (p) 3000 s, NCPCM (5%)
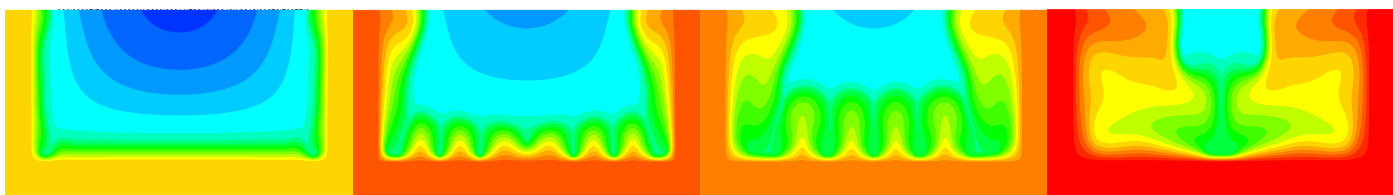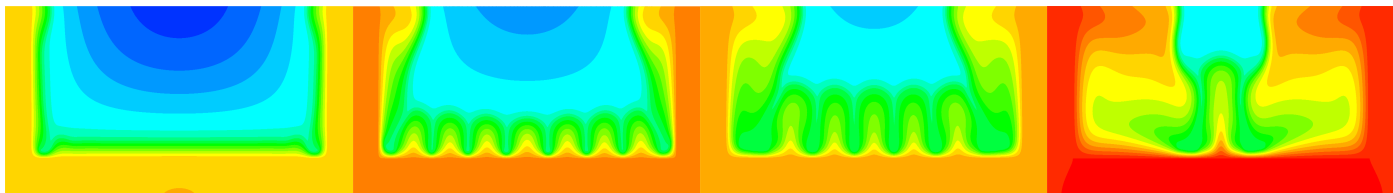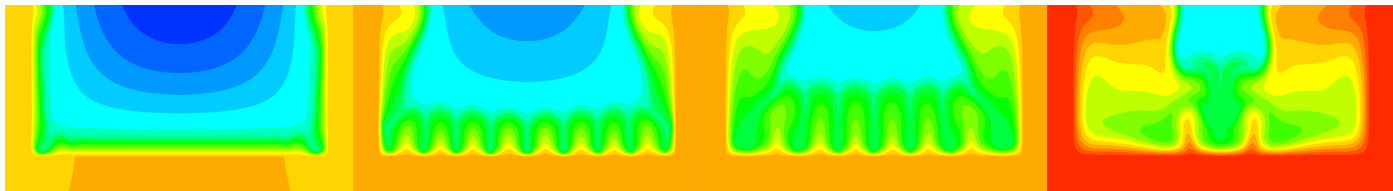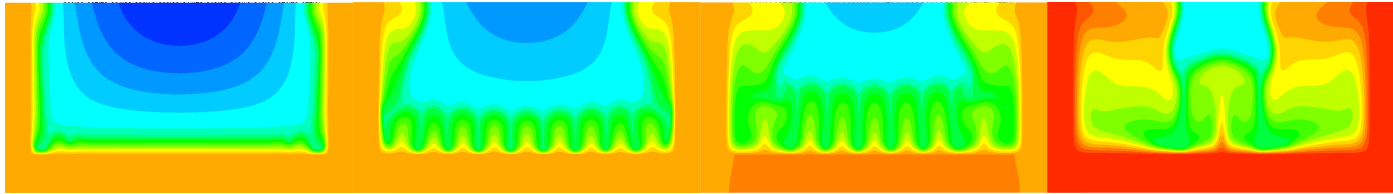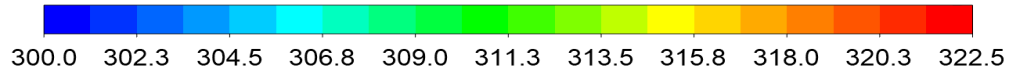
Figure 11: *Variation of isotherms contours at various t of PCM filled heat sink and various nanoparticles concentrations of NCPCM based heat sinks.*
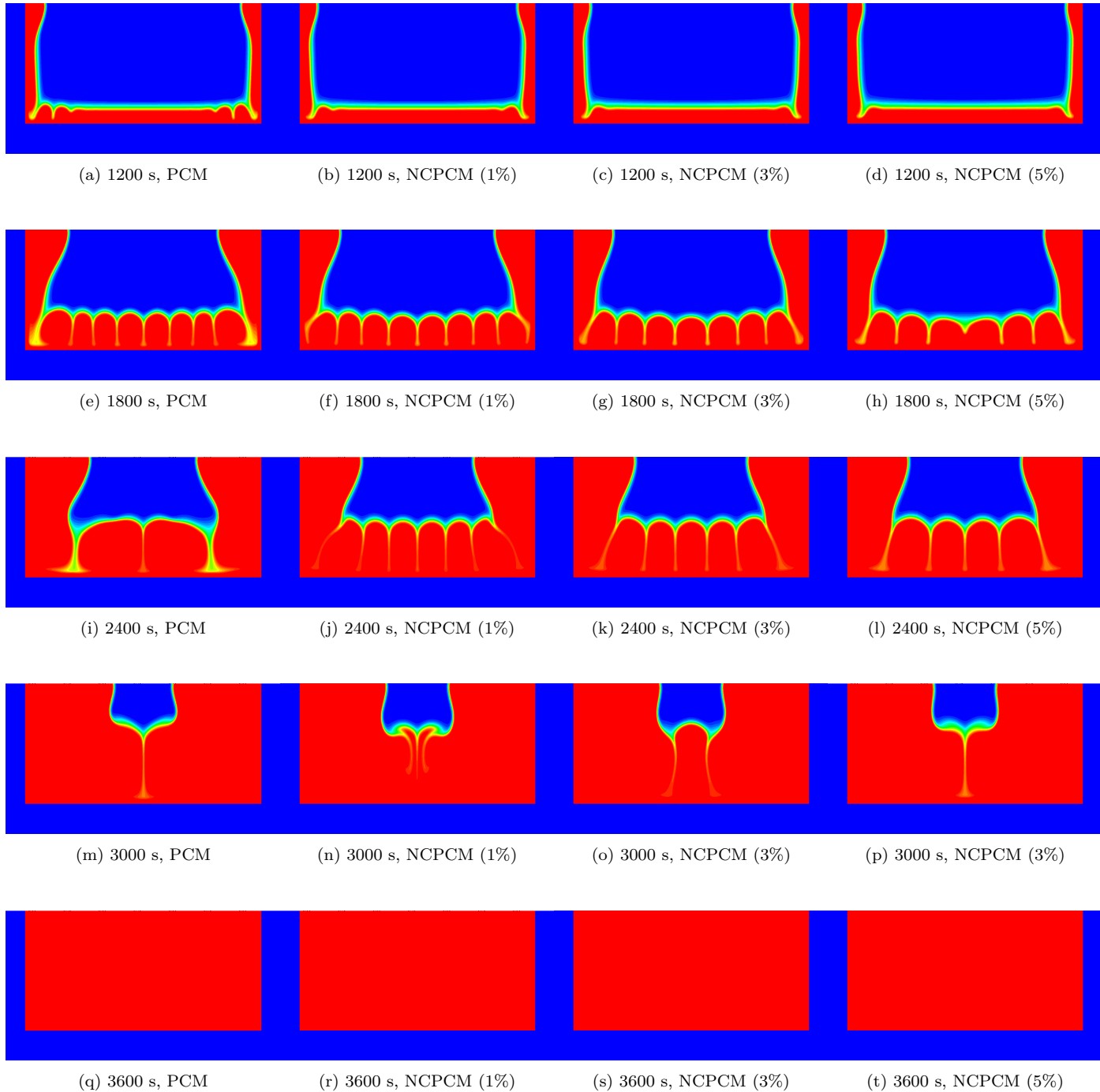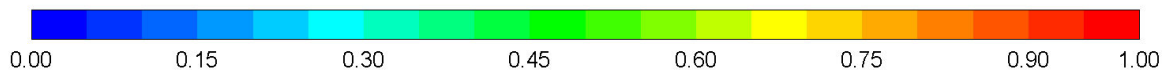
Figure 12: *Variation of f_l at various t of PCM filled heat sink and various nanoparticles concentrations of NCPCM based heat sinks.*

however it is decreased by -1.54%, -16.57%, and -27.64% by adding the Cu nanoparticles of 1%, 3%, and 5% concentration, respectively, in MF because of the increase of the total mass of PCM.

The comparison of MF+PCM and MF+NCPCM isotherms are further presented in Fig. 14 for different time intervals of 1200, 1800, 2400 and 3000 s. It can be seen that the temperature increases with the increase of time and with the increase of Cu nanoparticles φ. The MF provides a constant heat transfer path from bottom to top of the heat sink due to interconnected MF structure. Thus, the main contribution of heat transfer is because of heat conduction. In addition, nanoparticles have the higher thermal conductivity which further improve the heat transfer enhancement with the increase of added amount. A closer look reveals that in combination of nanoparticles and MF, the significance heat transfer contribution is because of the MF. Further more, the comparison of NCPCM and MF+NCPCM isotherms, shown in Figs. 11 and 14, respectively, reveals that the addition of MF in PCM provide a more uniform heat distribution compared to the NCPCM heat sink. Furthermore, Fig. 15 shows the f_l contours of MF+PCM and MF+NCPCM heat sink at different time periods of 1200, 1800, 2400 and 3000 s. The melting behaviour of PCM shows the uniform melting because of the addition of MF with increase of time. However, the higher f_l contours can be seen the addition of nanoparticles for each time step especially at 2400 s. The PCM melting improves as the φ increases from 1% to 5% because of the higher thermal conductivity of Cu nanoparticles. Since, the both MF and nanoparticles have the thermal conductivity, thus, improves the melting of the PCM resulting in lower t_{melt} and latent–heating phase is obtained. However, the higher heat transfer rate is achieved with the addition of MF. Therefore, by comparing the results, shown in Figs. 13b, 11 and 15, it can be suggested the nanoparticles having 1% volume fraction is enough in combination of MF embedded heat sink for effective thermal cooling performance.

4.7. Effect of different MF porosities with constant nanoparticles concentration

Fig. 16 illustrates the effect of varying MF porosities (85%, 90% and 95%) with a constant nanoparticles concentration of 5% and PPI of 10 at 5 W. The results of T_{HS} and f_l of PCM, NCPCM and MF+NCPCM heat sinks are presented in Fig. 16a. It can be revealed that lower T_{HS} is achieved initially before the complete melting of PCM for the cases of NCPCM and MF+NCPCM heat sinks which is due the effective heat transfer from the heat sink base towards ambient in presence of high thermal conductive nanoparticles

33
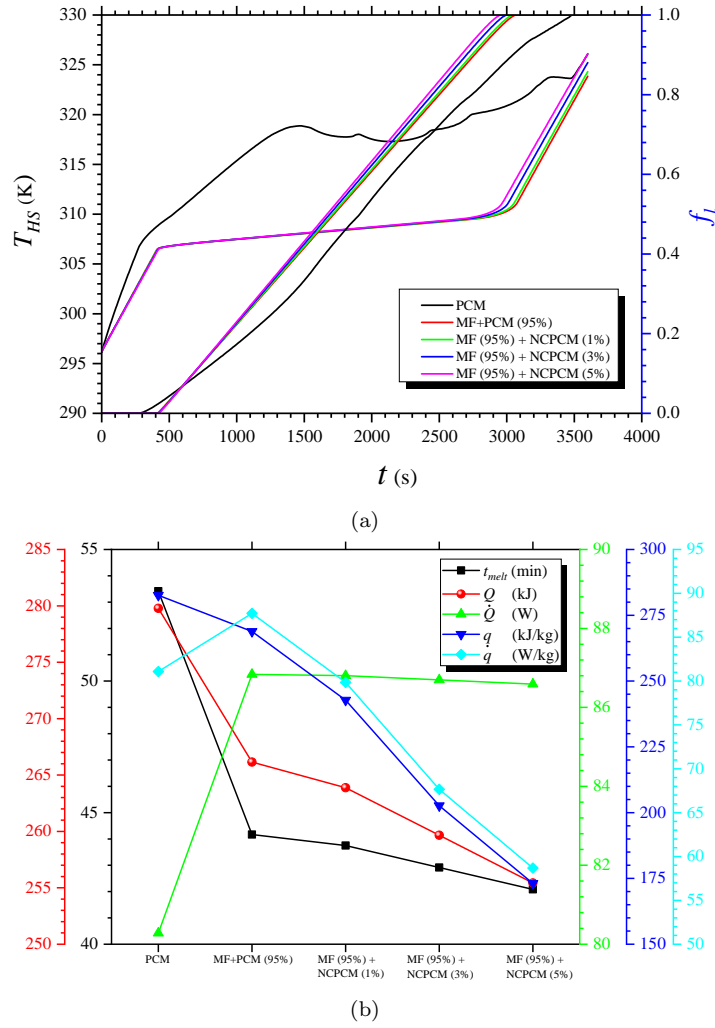
Figure 13: *Effect of different nanoparticles concentrations with constant MF+PCM based heat sink: (a) T_{HS} and f_l, (b) t_{melt}, Q, $\dot{Q}$, q and $\dot{q}$.*

and porous medium with PCM. However it can be seen that MF+NCPCM heat sink of 5% Cu concentration and 95% porosity has the lowest T_{HS} of 326.11 °C and higher latent–heating phase completion duration after 3600 s compared with the NCPCM (5%) heat sink. This reveals that a MF+PCM heat sink has the better thermal performance compared with PCM–only and NCPCM heat sinks. Similarly, higher f_l is obtained for MF+NCPCM heat sinks compared with PCM and NCPCM heats sink. However, a closer analysis presents that NCPCM heat sink has the higher f_l compared with PCM–only heat sink results in shorter the melting time of PCM. Moreover, a 95% porosity and 5% nanoparticles concentration heat sink has the lower f_l which takes the higher time to melt the PCM completely compared with 90% and 85% porosities MF+NCPCM heat sinks. The t_{melt} for PCM, NCPCM and MF+NCPCM of 95%, 90% and 85% porosities is obtained of 53.42, 52.17, 41.50, 40.08 and 38.83 mins, respectively, as shown in Fig. 16b. The reduction in t_{melt} is obtained of -2.34%,

Static Temperature

[k]   307.00   307.83   308.65   309.48   310.30   311.13   311.95   312.50

(a) 1200 s, MF+PCM   (b) 1800 s, MF+PCM   (c) 2400 s, MF+PCM   (d) 3000 s, MF+PCM

(e) 1200 s, MF+NCPCM (1%)   (f) 1800 s, MF+NCPCM (1%)   (g) 2400 s, MF+NCPCM (1%)   (h) 3000 s, MF+NCPCM (1%)

(i) 1200 s, MF+NCPCM (3%)   (j) 1800 s, MF+NCPCM (3%)   (k) 2400 s, MF+NCPCM (3%)   (l) 3000 s, MF+NCPCM (3%)

(m) 1200 s, MF+NCPCM (5%)   (n) 1800 s, MF+NCPCM (5%)   (o) 2400 s, MF+NCPCM (5%)   (p) 3000 s, MF+NCPCM (5%)
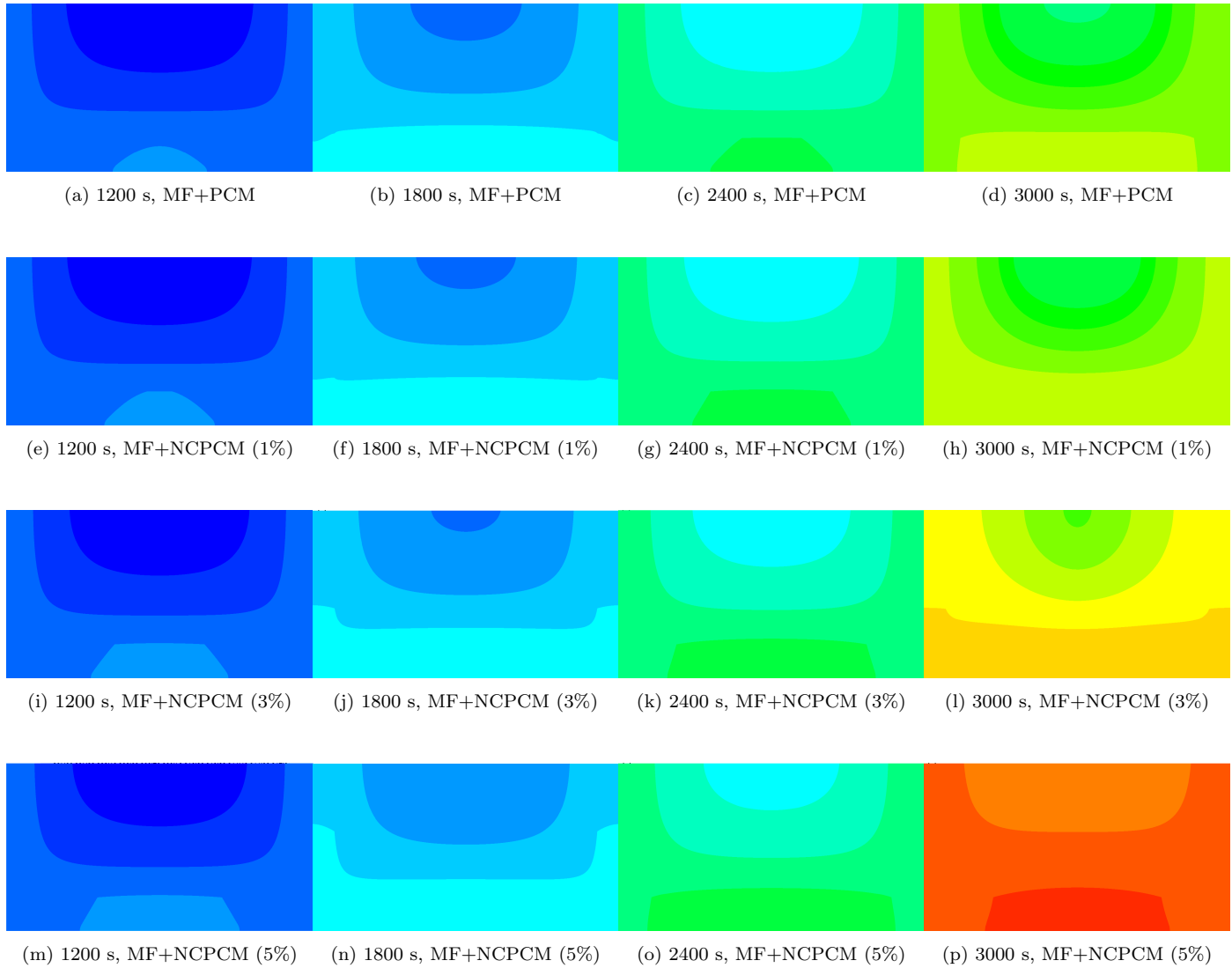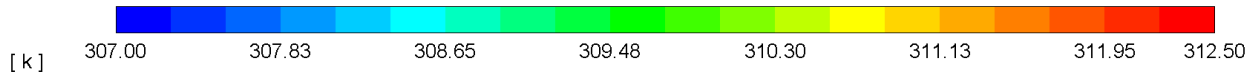
Figure 14: *Variation of isotherms at various t of MF+PCM and MF+NCPCM heat sink of different nanoparticles volume fractions.*
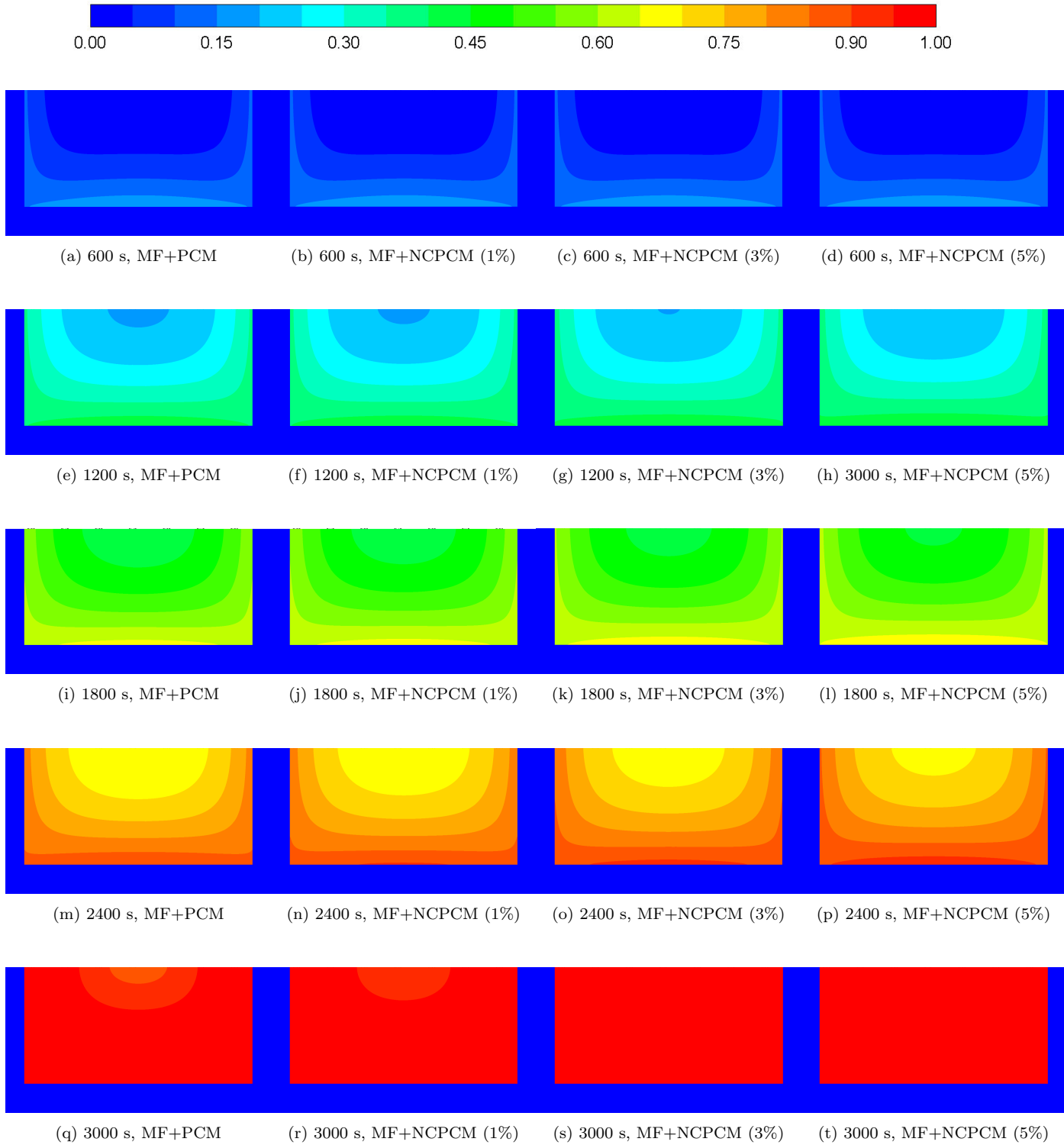
Figure 15: *Variation of f_l at various t of MF+PCM and MF+NCPCM heat sink of different nanoparticles volume fractions.*

−22.31%, −24.96%, and −27.30% for NCPCM, MF+NCPCM (95%), MF+NCPCM (90%), and MF+NCPCM (85%), respectively, compared with PCM filled heat sink. The results of Q and q reveal the decreasing trend for both NCPCM and MF+NCPCM filled heat sink compared with PCM filled heat sink. However, it can be observed that the variations in Q and q for MF+NCPCM heat sink cases are very less significant. The reduction in Q is achieved of −1.68%, −9.23%, −9.52%, and −9.64% for NCPCM, MF+NCPCM (95%), MF+NCPCM (90%), and MF+NCPCM (85%), respectively, compared with PCM filled heat sink. Similarly, the reduction in q is obtained of −34.04% for NCPCM heat sink, however, a slight decrease is obtained of −39.10%, −39.30%, and −39.38% for MF+NCPCM heat sink of 95%, 90%, and 85% porosities, respectively, compared with PCM filled heat sink case. Fig. 16b, a increasing trend is observed in $\dot{Q}$ for NCPCM and MF+NCPCM heat sinks. A slight enhancement of 0.19% for NCPCM heat sink, however, a sharp enhancement of 7.97%, 10.44%, and 12.85% is obtained for MF+NCPCM heat sink of 95%, 90%, and 85% porosities, respectively, compared with PCM filled heat sink. Comparably, the reduction in $\dot{q}$ results is obtained of −32.79%, −27.57%, −25.91%, and −24.28% for NCPCM, MF+NCPCM (95%), MF+NCPCM (90%), and MF+NCPCM (85%), respectively, compared with PCM filled heat sink. The result illustrates that only NCPCM heat sink reduced the q and $\dot{q}$ more significantly as compared to MF+NCPCM heat sink. Since, the q and $\dot{q}$ depend on the mass of the PCM which means that more the PCM mass more the decrease in q and $\dot{q}$ or vice versa.

5. Concluding remarks and suggestions

The present study explores the parametric investigation of a two-dimensional (2D) heat sink filled up with the composite of PCM, NCPCM, MF+PCM and MF+NCPCM through numerical approach. The influence of Cu nanoparticles is evaluated by varying the volume fraction with PCM and MFs. The effect of different parameters such as different MF materials, porosities, pore densities, volume fractions of NCPCM, combination of MF+NCPCM by varying different porosities and nanoparticles volume fractions, and power levels. The contours of liquid–fraction and isotherms are presented at different time periods and volume fractions of Cu nanoparticles. Thermal performance of heat sink is evaluated using different performance indicators such as melting time, heat storage capacity, heat storage density, rate of heat transfer, and rate of heat transfer density. The key findings from results are identified as follows:

37
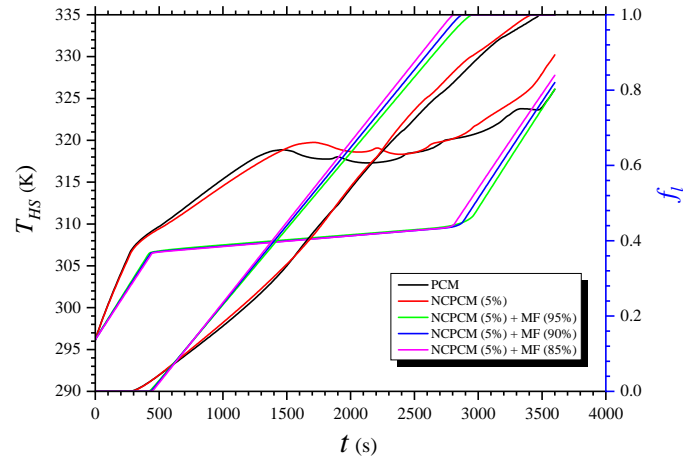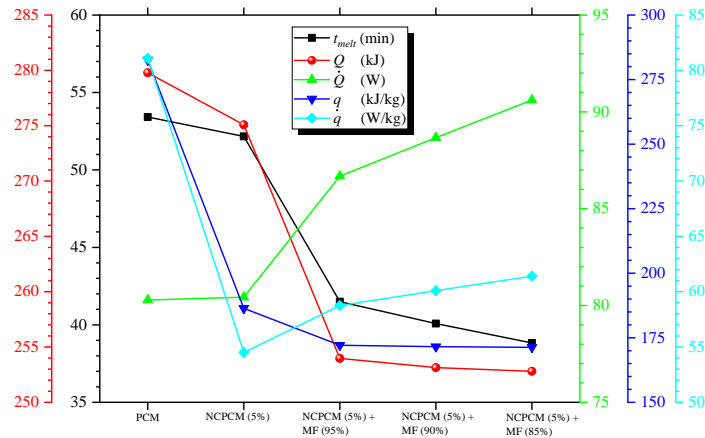
Figure 16: *Effect of different MF porosities with constant nanoparticles concentration NCPCM based heat sink: (a) T_{HS} and f_l, (b) t_{melt}, Q, $\dot{Q}$, q and $\dot{q}$.*

- A uniform heating and melting of PCM is observed b by embedding the MF with PCM filled heat sink. The lower heat sink temperature and enhanced melting rate is obtained by Cu MF followed by Al and Ni MFs. The higher heat transfer rate of 86.84 W and lowest melting time of 44.17 min are obtained Cu MF+PCM embedded heat sink.

- The melting time and latent–heating phase duration were decreased with the increase of power level. However, the rate of heat transfer increased with the increase of power level.

- The pore size showed a slight variation in reduction of heat sink temperature and melting of PCM. However, the 10 PPI showed the lower heat sink temperature and higher melting time. In addition, the comparison of porosities revealed the highest porosity of 95% showed the lowest heat sink temperature and liquid–fraction of PCM.

The higher reduction melting time and heat storage capacity were obtained of -17.32% and -4.87%, respectively, however, lower rate of heat transfer was increased of 8.16% with 95% porosity and 10 PPI Cu MF+PCM based heat sink.

- There are less significance effects observed by adding the nanoparticles inside the PCM in reduction of heat sink and PCM temperatures. The lower heat sink and NCPCM temperatures were achieved with the increase of volume fraction of nanoparticles. The addition of nanoparticles improved the thermal conductivity and viscosity of PCM with the increase of volume fraction and improved the uniformity in melting process. The melting time was reduced by -1.25%, -1.87% and -2.34% with the addition of 1%, 3% and 5% volume fraction of Cu nanoparticles. Increasing trend was observed in heat storage capacity and rate of heat transfer at 1% volume fraction of Cu nanoparticles. Later on, they were decreased. A rapid decrease in heat storage density and rate of heat transfer density was obtained. The rate of heat storage is enhanced by 1.35%, 0.76%, and 0.19% by adding 1%, 3% and 5% volume concentration of Cu nanoparticles, respectively, compared with the PCM filled heat sink case.

- The addition of nanoparticles enhanced the melting rate and thermal conduction mode of PCM with the increase of volume fraction because of the enhancement in effective thermal conductivity and viscous effects of NCPCM. Addition of nanoparticles improved the uniformity in melting process.

- With the addition of the NCPCM and MF, lower heat sink temperature and higher liquid–fraction were obtained. Additionally, the latent–heating phase duration was decreased with the increase of Cu nanoparticles volume fraction. The reduction in melting time was obtained of -18.10%, -19.66% and -21.22% by adding the 1%, 3% and 5% volume fraction of Cu nanoparticles with 95% porous Cu MF. Higher rate of heat transfer of 8.12% was obtained at 1% volume fraction of Cu nanoparticles. However, a sharp decrease in heat storage density and rate of heat transfer density because of increase in total mass of the PCM due to addition of nanoparticles. A uniform temperature distribution and melting phenomenon was observed through isotherms and liquid–fraction contours.

- The different porosities (85%, 90% and 95%) of MF with constant volume fraction of 5% revealed that lower heat sink temperature and higher latent–heating phase

39

completion duration. The lower liquid–fraction was obtained with 95% porous of MF and 5% volume fraction of Cu nanoparticles. The reduction in melting time was obtained of -2.34%, -22.31%, -24.96% and -27.30% for for NCPCM, MF+NCPCM (95%), MF+NCPCM (90%), and MF+NCPCM (85%), respectively, compared with PCM–only case. The slight improvement of 0.19% for NCPCM heat sink, however, a sharp enhancement of 7.97%, 10.44%, and 12.85% is obtained for NCPCM/MF+PCM heat sink of 95%, 90%, and 85% porosities, respectively, compared with pure PCM filed heat sink.

After carefully analysis of the pure PCM, NCPCM, MF+PCM and MF+NCPCM based heat sink, it can been reveal that optimum heat transfer rate and heat absorption capacity are obtained at 1% of Cu nanoparticles concentration with 95% porosity and 10 PPI Cu MF heat sink for efficient thermal cooling performance of electronic devices.

Conflict of interest

The authors declare no conflict of interest regarding this research article.

References

[1] SM Sohel Murshed. *Advanced Cooling Technologies and Applications*. BoD–Books on Demand, 2019.

[2] LT Yeh. Review of heat transfer technologies in electronic equipment. *Journal of electronic packaging*, 117(4):333–339, 1995.

[3] S.M. Sohel Murshed and C.A. Nieto de Castro. A critical review of traditional and emerging techniques and fluids for electronics cooling. *Renewable and Sustainable Energy Reviews*, 78:821–833, oct 2017.

[4] Adeel Arshad, Mark Jabbal, Yuying Yan, and Jo Darkwa. The micro-/nano-PCMs for thermal energy storage systems: A state of art review. *International Journal of Energy Research*, 43(11):5572–5620, may 2019.

[5] Muhammad Junaid Ashraf, Hafiz Muhammad Ali, Hazrat Usman, and Adeel Arshad. Experimental passive electronics cooling: Parametric investigation of pin-fin geometries and efficient phase change materials. *International Journal of Heat and Mass Transfer*, 115:251–263, dec 2017.

[6] Adeel Arshad, Hafiz Muhammad Ali, Muzaffar Ali, and Shehryar Manzoor. Thermal performance of phase change material (PCM) based pin-finned heat sinks for electronics devices: Effect of pin thickness and PCM volume fraction. *Applied Thermal Engineering*, 112:143–155, feb 2017.

[7] Hafiz Muhammad Ali and Adeel Arshad. Experimental investigation of n-eicosane based circular pin-fin heat sinks for passive cooling of electronic devices. *International Journal of Heat and Mass Transfer*, 112:649–661, sep 2017.

[8] Adeel Arshad, Hafiz Muhammad Ali, Wei-Mon Yan, Ahmed Kadhim Hussein, and Majid Ahmadlouydarab. An experimental study of enhanced heat sinks for thermal management using n-eicosane as phase change material. *Applied Thermal Engineering*, 132:52–66, mar 2018.

[9] Santosh Kumar Sahoo, Mihir Kumar Das, and Prasenjit Rath. Application of TCE-PCM based heat sinks for cooling of electronic components: A review. *Renewable and Sustainable Energy Reviews*, 59:550–582, jun 2016.

41

[10] Adeel Arshad, Mark Jabbal, and Yuying Yan. Thermal performance of PCM-based heat sink with partially filled copper oxide coated metal-foam for thermal management of microelectronics. In *2020 19th IEEE Intersociety Conference on Thermal and Thermomechanical Phenomena in Electronic Systems (ITherm)*. IEEE, jul 2020.

[11] Adeel Arshad, Mark Jabbal, and Yuying Yan. Preparation and characteristics evaluation of mono and hybrid nano-enhanced phase change materials (NePCMs) for thermal management of microelectronics. *Energy Conversion and Management*, 205:112444, feb 2020.

[12] Adeel Arshad, Mark Jabbal, and Yuying Yan. Thermophysical characteristics and application of metallic-oxide based mono and hybrid nanocomposite phase change materials for thermal management systems. *Applied Thermal Engineering*, 181:115999, nov 2020.

[13] Adeel Arshad, Mark Jabbal, Lei Shi, Jo Darkwa, Nicola J. Weston, and Yuying Yan. Development of TiO2/RT–35hc based nanocomposite phase change materials (NCPCMs) for thermal management applications. *Sustainable Energy Technologies and Assessments*, page 100865, dec 2020.

[14] Saad Mahmoud, Aaron Tang, Chin Toh, Raya AL-Dadah, and Sein Leung Soo. Experimental investigation of inserts configurations and PCM type on the thermal performance of PCM based heat sinks. *Applied Energy*, 112:1349–1356, dec 2013.

[15] Simone Mancin, Andrea Diani, Luca Doretti, Kamel Hooman, and Luisa Rossetto. Experimental analysis of phase change phenomenon of paraffin waxes embedded in copper foams. *International Journal of Thermal Sciences*, 90:79–89, apr 2015.

[16] C.Y. Zhao, W. Lu, and Y. Tian. Heat transfer enhancement for thermal energy storage using metal foams embedded within phase change materials (PCMs). *Solar Energy*, 84(8):1402–1412, aug 2010.

[17] Y. Tian and C.Y. Zhao. A numerical investigation of heat transfer in phase change materials (PCMs) embedded in porous metals. *Energy*, 36(9):5539–5546, sep 2011.

[18] Sriharsha S. Sundarram and Wei Li. The effect of pore size and porosity on thermal management performance of phase change material infiltrated microcellular metal foams. *Applied Thermal Engineering*, 64(1-2):147–154, mar 2014.

[19] Zhenqian Chen, Dongyan Gao, and Juan Shi. Experimental and numerical study on melting of phase change materials in metal foams at pore scale. *International Journal of Heat and Mass Transfer*, 72:646–655, may 2014.

[20] S.A. Nada and W.G. Alshaer. Comprehensive parametric study of using carbon foam structures saturated with PCMs in thermal management of electronic systems. *Energy Conversion and Management*, 105:93–102, nov 2015.

[21] W.G. Alshaer, S.A. Nada, M.A. Rady, Cedric Le Bot, and Elena Palomo Del Barrio. Numerical investigations of using carbon foam/PCM/nano carbon tubes composites in thermal management of electronic equipment. *Energy Conversion and Management*, 89:873–884, jan 2015.

[22] Morteza Alipanah and Xianglin Li. Numerical studies of lithium-ion battery thermal management systems using phase change materials and metal foams. *International Journal of Heat and Mass Transfer*, 102:1159–1168, nov 2016.

[23] P. Zhang, Z.N. Meng, H. Zhu, Y.L. Wang, and S.P. Peng. Melting heat transfer characteristics of a composite phase change material fabricated by paraffin and metal foam. *Applied Energy*, 185:1971–1983, jan 2017.

[24] Jasim M. Mahdi and Emmanuel C. Nsofor. Melting enhancement in triplex-tube latent heat energy storage system using nanoparticles-metal foam combination. *Applied Energy*, 191:22–34, apr 2017.

[25] Jasim M. Mahdi and Emmanuel C. Nsofor. Solidification enhancement in a triplex-tube latent heat energy storage system using nanoparticles-metal foam combination. *Energy*, 126:501–512, may 2017.

[26] Bernardo Buonomo, Davide Ercole, Oronzio Manca, and Sergio Nardini. Numerical analysis on a latent thermal energy storage system with phase change materials and aluminum foam. *Heat Transfer Engineering*, 41(12):1075–1084, apr 2019.

[27] Ali Chamkha, Ali Veismoradi, Mohammad Ghalambaz, and Pouyan Talebizadehsardari. Phase change heat transfer in an l-shape heatsink occupied with paraffin-copper metal foam. *Applied Thermal Engineering*, 177:115493, aug 2020.

[28] Zhixiong Li, Amin Shahsavar, Abdullah A.A.A. Al-Rashed, and Pouyan Talebizadehsardari. Effect of porous medium and nanoparticles presences in a counter-current triple-tube composite porous/nano-PCM system. *Applied Thermal Engineering*, 167:114777, feb 2020.

[29] Jasim M. Mahdi, Hayder I. Mohammed, Emad T. Hashim, Pouyan Talebizadehsardari, and Emmanuel C. Nsofor. Solidification enhancement with multiple PCMs, cascaded metal foam and nanoparticles in the shell-and-tube energy storage system. *Applied Energy*, 257:113993, jan 2020.

[30] Adeel Arshad, Mark Jabbal, Pouyan Talebizadeh Sardari, Muhammad Anser Bashir, Hamza Faraji, and Yuying Yan. Transient simulation of finned heat sinks embedded with PCM for electronics cooling. *Thermal Science and Engineering Progress*, 18:100520, aug 2020.

[31] Adeel Arshad, Mohammed Ibrahim Alabdullatif, Mark Jabbal, and Yuying Yan. Towards the thermal management of electronic devices: A parametric investigation of finned heat sink filled with PCM. *International Communications in Heat and Mass Transfer*, 129:105643, dec 2021.

[32] Hayder I. Mohammed, Pouyan Talebizadehsardari, Jasim M. Mahdi, Adeel Arshad, Adriano Sciacovelli, and Donald Giddings. Improved melting of latent heat storage via porous medium and uniform joule heat generation. *Journal of Energy Storage*, 31:101747, oct 2020.

[33] V. V. Calmidi and R. L. Mahajan. Forced convection in high porosity metal foams. *Journal of Heat Transfer*, 122(3):557–565, feb 2000.

[34] Ravikanth S. Vajjha and Debendra K. Das. Experimental determination of thermal conductivity of three nanofluids and development of new correlations. *International Journal of Heat and Mass Transfer*, 52(21-22):4675–4682, oct 2009.

[35] A. Valan Arasu and Arun S. Mujumdar. Numerical study on melting of paraffin wax with al2o3 in a square enclosure. *International Communications in Heat and Mass Transfer*, 39(1):8–16, jan 2012.

[36] Jasim M. Mahdi and Emmanuel C. Nsofor. Melting enhancement in triplex-tube latent thermal energy storage system using nanoparticles-fins combination. *International Journal of Heat and Mass Transfer*, 109:417–427, jun 2017.

[37] B.P. Leonard. A stable and accurate convective modelling procedure based on quadratic upstream interpolation. *Computer Methods in Applied Mechanics and Engineering*, 19(1):59–98, jun 1979.

[38] Suhas Patankar. *Numerical heat transfer and fluid flow*. Hemisphere Publishing Corporation; McGraw-Hill Book Company, New York., 2018.

[39] Yang Xu, Qinlong Ren, Zhang-Jing Zheng, and Ya-Ling He. Evaluation and optimization of melting performance for a latent heat thermal energy storage unit partially filled with porous media. *Applied Energy*, 193:84–95, may 2017.

[40] Zhenyu Liu, Yuanpeng Yao, and Huiying Wu. Numerical modeling for solid–liquid phase change phenomena in porous media: Shell-and-tube type latent heat thermal energy storage. *Applied Energy*, 112:1222–1232, dec 2013.

[41] Jasim M. Mahdi, Hayder I. Mohammed, Pouyan Talebizadehsardari, Mohammad Ghalambaz, Hasan Sh. Majdi, Afrasyab khan, Wahiba Yaci, and Donald Giddings. Simultaneous and consecutive charging and discharging of a PCM-based domestic air heater with metal foam. *Applied Thermal Engineering*, 197:117408, oct 2021.

[42] Pouyan Talebizadeh Sardari, Hayder I. Mohammed, Donald Giddings, Gavin S. walker, Mark Gillott, and David Grant. Numerical study of a multiple-segment metal foam-PCM latent heat storage unit: Effect of porosity, pore density and location of heat source. *Energy*, 189:116108, dec 2019.

Nomenclature

Abbreviations

Al	Aluminum
Cu	Copper
FVM	Finite volume method
HS	Heat sink
NCPCM	Nanocomposite phase change material
Ni	Nickel
DFBM	Darcy-Forchheimer-Brinkman model
LTE	Local thermal equilibrium
LTNE	Local thermal non-equilibrium
PCMs	Phase change materials
PPI	Pores per inch
TM	Thermal management
UDF	User–defined function

Symbols

A_m	Mushy zone
B	Boltzman constant (J/K)
ρc_p	Volumetric heat capacity ($J/m^3.K$)
C_F	Inertial coefficient
K	Permeability
d_l	Ligament or cell diameter (m)
d_p	Pore diameter or pore size (m)
g	Gravitational acceleration (m/s^2)
H	Height (mm)
Q	Heat storage capacity (J)
q	Heat storage density (J/Kg)
k	Thermal conductivity ($W/m.K$)
L	Latent heat of fusion ($J/kg.K$)
m	Mass (Kg)
p	Pressure (Pa)
$\dot{Q}$	Rate of heat transfer (W)

$\dot{q}$	Rate of heat transfer density (W/Kg)
q'''	Volumetric heat generation (W/m^3)
S	Source term in momentum equation
T	Temperature (K)
t	Time (sec)
u	Velocity component in $x-$axis (m/s)
v	Velocity component in $y-$axis (m/s)
W	Width (mm)
c_p	Specific heat capacity ($J/kg.K$)
ΔH	Fractional latent-heat ($J/kg.K$)
$2D$	Two dimensional

Greek letters

φ	Volume fraction
β	Thermal expansion coefficient (1/K)
μ	Viscosity (Pa.s)
f_l, λ	Liquid fraction
ε	Porosity
ω	Pore density

Subscripts

HS	Heat sink
hs	Heat source
ini	Initial
l	Liquidus
m	Melting
mf	Metal-foam
$ncpcm$	Nanocomposite phase change material
np	Nanoparticles
ref	Reference
x	$x-$axis
y	$y-$axis

Table 1: Thermophysical properties of PCM, nanoparticles, and MFs [10, 28, 36].

Physical properties	RT–35HC	Nanoparticles (Cu)	Metal-foam (Al)	Metal-foam (Cu)	Metal-foam (Ni)
T_m (K)	308	-	-	-	-
T_s (K)	307	-	-	-	-
T_l (K)	309	-	-	-	-
L (kJ/kg)	240	-	-	-	-
k (W/m.K)	0.2	400	202.4	400	91
c_p (J/kg.K)	2000	380	871	385	440
ρ (kg/m³)	880 (solid) 770 (liquid)	8920	2719	8960	8902
β (1/K)	0.0006	-	-	-	-

Table 2: Grid independence analysis.

Number of elements	Melting Time	Deviation (%)	Total energy (kJ/kg)	Deviation (%)
43753	1290	0.00	242.47	0.00
48305	1300	0.78	242.34	0.05
54087	1295	0.38	242.49	0.06
60796	1295	0.00	242.39	0.04